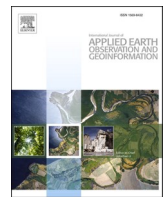




Contents lists available at ScienceDirect

International Journal of Applied Earth Observation and Geoinformation

journal homepage: www.elsevier.com/locate/jag



Developing an annual global Sub-National scale economic data from 1992 to 2021 using nighttime lights and deep learning

Hang Zhang ^{a,b,c}, Guanpeng Dong ^{a,b,c,*}, Bing Li ^c, Zunyi Xie ^b, Changhong Miao ^{a,b,c}, Fan Yang ^c, Yang Gao ^a, Xiaoyu Meng ^c, Dongyang Yang ^c, Yong Liu ^c, Hongjuan Zhang ^c, Leying Wu ^a, Fanglin Shi ^c, Yulong Chen ^c, Wenjie Wu ^d, Edyta Laszkiewicz ^e, Yutian Liang ^f, Binbin Lu ^g, Jing Yao ^h, Xuecao Li ⁱ

^a Climate Change and Carbon Neutrality Lab, Henan University, Kaifeng, 475001, China

^b College of Geography and Environmental Science, Henan University, Kaifeng 475001, China

^c Key Research Institute of Yellow River Civilization and Sustainable Development, Henan University, Kaifeng 475001, China

^d School of Urban Design, Wuhan University, Wuhan, China

^e Faculty of Economics and Sociology, University of Lodz, Lodz, Poland

^f School of Geography and Planning, Sun Yat-sen University, Guangzhou, China

^g School of Remote Sensing and Information Engineering, Wuhan University, Wuhan, China

^h Department of Urban Studies, University of Glasgow, Glasgow, the UK

ⁱ College of Land Science and Technology, China Agricultural University, Beijing, China



ARTICLE INFO

Keywords:

GDP per capita
Economic assessment
Nighttime lights
Multi-layer perceptron
Spatial spillover
Scale effects
Light gradient boosting machine

ABSTRACT

The Gross Domestic Product (GDP) per capita is one of the most widely used socioeconomic indicators, serving as an integral component for climate change impact analysis. However, a national scale assessment may induce considerable bias because it conceals any internal variations within a country. The lack of a long-term sub-national scale GDP data is a substantive hindrance. Leveraging the close relationship between nighttime lights and GDP, we address this gap by developing a novel methodological framework in two steps. First, under the modeling philosophy of spatial statistics, we developed a novel approach based on deep and machine learning techniques to establish a complex mapping between two inconsistent nighttime lights (NTL) datasets: the Defense Meteorological Satellite Program's Operational Linescan System (DMSP) and the National Polar-Orbiting Partnership's Visible Infrared Imaging Radiometer Suite (VIIRS). The models achieve accuracies ranging from 0.945 to 0.980 (correlation coefficients). By taking the estimations ensemble of the two techniques, the time series of DMSP data was extended to 2021. Next, a novel modeling strategy based on multi-layer perceptron was developed to derive the non-linear relationship between NTL and GDP per capita at sub-national scale to alleviate scale effects at this granularity, while explicitly capturing regional heterogeneity effect. The trained models achieve average accuracies of 0.967, 0.959, and 0.959 on the training, validation, and test sets, respectively. We evaluate the developed dataset at the global, national, and sub-national scales from various perspective, and the results offer solid evidence on the reliability of the estimated economic data. By linking to historical global climate change data, we quantify global economic losses attributed to extreme heat to demonstrate how the estimated GDP data can be useful in the climate change impact analysis.

1. Introduction

Gross Domestic Product (GDP) and GDP per capita are paramount socio-economic indicators in development, policy-making, and management analysis, as they offer comprehensive and comparable metrics of economic development of nations or regions over a period (Geiger,

2018; Nordhaus, 1991; Chen and Nordhaus, 2011). The World Bank and other organizations have compiled long-term national scale economic data, forming the empirical basis for evaluating interactions between human activities and nature. For instance, the past, contemporary, and projected future economic losses linked to both existing and projected climate change have been assessed at the national scale (Bowen et al.,

* Corresponding author at: Climate Change and Carbon Neutrality Lab, Henan University, Kaifeng 475001, China.

E-mail address: gpdong@vip.henu.edu.cn (G. Dong).

<https://doi.org/10.1016/j.jag.2024.104086>

Received 4 January 2024; Received in revised form 18 July 2024; Accepted 5 August 2024

Available online 16 August 2024

1569-8432/© 2024 The Author(s). Published by Elsevier B.V. This is an open access article under the CC BY-NC license (<http://creativecommons.org/licenses/by-nc/4.0/>).

2012; Fankhauser & Jotzo, 2018; Nordhaus, 2019). However, such national-scale assessments can introduce biases by obscuring intra-country variabilities in both economic and climate change dynamics (Kalkuhl & Wenz, 2020). Therefore, there is an urgent demand for more granular spatial assessments of economic loss to support the United Nations sustainable development goals (SDGs), particularly in understanding the heterogeneous effects of losses within countries.

In the context of climate change, to date, owing to the lack of reliable sub-national-scale economic data, there has been a limited number of studies focusing on global sub-national scale economic risk assessment (Kalkuhl & Wenz, 2020; Kotz et al., 2021). Official statistics have been the key and highly-regarded data sources for compilation of GDP and its derivatives such as GDP per capita or economic grow rates, however, roughly 70 % of economic statistics for sub-national unit-year pairs are missing due to various reasons (Kalkuhl & Wenz, 2020). For developing and poor countries, the issue of data paucity is much exacerbated (Chen & Nordhaus, 2011; Henderson et al., 2012). Discrepancies in accounting methods for economic output between countries and changes in accounting methods over time can also result in decreased cross-country comparability (Deaton, 2001; Pinkovskiy & Sala-i-Martin, 2016). Altogether, official statistics could introduce non-negligible bias into economic risk assessment.

Global gridded GDP data has been synthesized by formulating various mathematical conversion functions, bridging high-resolution raster-based proxy variables with national-scale economic data (Chen et al., 2022; Wang & Sun, 2022). Methods for establishing relationships between proxy variables (typically nighttime lights or population) and economic data fall into two categories: redistribution and model-fitting approaches. The redistribution method allocates national economic data to units at a finer scale by calculating the share of proxy variables. Kummu et al. advance this approach and disaggregate sub-national-scale GDP onto grids using population as weights, which to some extent improve the reliability of data at the sub-national scale (Kummu et al., 2018). *Nonetheless, the redistribution method, at essence, is a linear decomposition that may obscure potential nonlinear relationship between proxy variables and economic indicators.*

Model-fitting methods, in contrast, derive finer-scale economic data by establishing linear or nonlinear functions that relate economic data to proxy variables. In particular, gridded GDP is estimated by establishing a relationship between nighttime lights (NTL) and GDP at the national scale (Chen et al., 2022). It is essential to acknowledge the inherent uncertainty or inconsistency across different spatial scales because of the modifiable areal unit problem (MAUP) (Fotheringham & Wong, 1991; Janelle et al., 2004) or scale effects (Dong et al., 2018; Dong and Harris, 2015; Zheng et al., 2023; Shi et al., 2023), which can compromise the quality and credibility of these gridded GDP datasets. Moreover, economic statistics make perfect sense for administrative units (ideally at fine spatial scales) in terms of policy evaluation and resource allocation, but their applicability on grids is less straightforward. This highlights a fundamental tradeoff in remote sensing application: the need to balance the pursuit of high spatiotemporal resolution with the practicality and relevance for socioeconomic policy-making.

NTL offers global-scale, long-term observations of artificial and natural light intensity during nighttime, offering a detailed overview of anthropogenic activities on Earth's surface (Chen et al., 2017; Li et al., 2020; Sánchez de Miguel et al., 2021). It has been increasingly used to estimate various socioeconomic variables such as GDP, population, poverty, urban, and energy consumption (Yu et al., 2015; Bennett & Smith, 2017; McCord & Rodriguez-Heredia, 2022; Zhou et al., 2014, 2022), since the seminal work of Chen and Nordhaus (2011) and Henderson et al. (2012), which first linked national economic growth to

NTL. There are two main types of NTL: the Defense Meteorological Satellite Program's Operational Linescan System (DMSP-OLS, DMSP) and the National Polar-Orbiting Partnership's Visible Infrared Imaging Radiometer Suite (NPP-VIIRS, VIIRS). Although both NTL datasets are acknowledged as effective proxies for detecting the dynamics of socio-economic activities (Yang et al., 2019), there are substantial inconsistencies that exist between them (Cui et al., 2021; Elvidge et al., 2013), presenting a major obstacle in long-term time series studies (Chen et al., 2021). Methods for integrating the two NTL datasets, such as kernel density transformation (Li et al., 2020; Wu et al., 2022), and geographically weighted approaches (Zheng et al., 2019), have highlighted the importance of neighborhood information. Kernel density and geographically weighted approaches assumes spatial stability and isotropy, thereby reducing multidimensional neighborhood information to one-dimensional neighborhood information, which may lead to information loss. These methods are based on the blooming effect of the DMSP, which is similar to the spillover effect in the spatial modeling literature (Townsend & Bruce, 2010), and therefore, deep learning and machine learning models can be constructed based on the spatial statistical modeling philosophy to flexibly handle neighborhood information.

Specifically, multi-layer perceptron (MLP) and Light Gradient Boosting Machine (LightGBM) algorithms are adept at capturing complex relationships due to their ability to handle nonlinearities and interactions (Goodfellow et al., 2016; Ke et al., 2017). MLP refines the nonlinear relationships between features through its multilayered architecture (Goodfellow et al., 2016), while LightGBM enhances decision tree construction with its gradient boosting mechanism, facilitating the capture of intricate patterns and local dependencies within the data (Chen & Guestrin, 2016; Ke et al., 2017). Such flexibility ensures that neighborhood information can be effectively integrated into the model. Additionally, compared to more complex convolutional neural networks, MLP and LightGBM offer expedited training and prediction capabilities due to their simpler structures, providing substantial computational benefits for processing global datasets. This is crucial for studies requiring bootstrapping- or permutation-based uncertainty quantification of DMSP-like nighttime lights data and relying on the SHapley Additive exPlanations (SHAP) method to analyze feature importance (Lundberg & Lee, 2017).

The present study leverages the relationship between nighttime lights and GDP—may it be linear or complex nonlinear—to develop a long-term annual global sub-national scale economic data. We first develop MLP and LightGBM models to reconstruct the precise mapping relationship between the VIIRS neighborhood information and DMSP data under the modeling philosophy of spatial statistics. SHAP-based feature importance analysis shows that neighborhood information contributes significantly to the final prediction outcomes and improves prediction accuracy through balancing positive and negative contributions among features. In the second step, based on the compiled DMSP data and official statistics based sub-national GDP data (with a large proportion of missing values), we train a MLP model to derive the nonlinear relationship between NTL and GDP per capita at the sub-national scale to alleviate the MAUP issue, while explicitly capturing both the spatial clustering effects by incorporating a spatial lag term of NTL, and the regional heterogeneity effects by recognizing the hierarchical nature of data. Finally, we verify the reliability of the estimated per capita GDP from multiple dimensions and investigate the impact of extreme high temperatures on economic growth utilizing a cutting-edge climate change econometric model. Empirical results show that the estimated sub-national scale GDP per capita data can contribute to more accurate assessment of economic loss due to climate change.

2. Identifying the data gap

To measure economic growth trends, data on economic output spanning 1992–2016 at the sub-national scale were collected, referred to as GDP per capita, for 1537 provinces, states, or regions in 76 countries (Kalkuhl & Wenz, 2020). To ensure comparability, economic data were converted from country-specific currencies to US dollars (USD) using exchange rates from the Federal Reserve Economic Data (FRED) database. Consequently, a global sub-national economic activity dataset in current US dollars comprising 25,989 samples was compiled (Kalkuhl & Wenz, 2020), offering a relatively large sample to establish a quantitative conversion relationship between NTL and GDP per capita at the sub-national scale. The information regarding the global NTL data and other auxiliary data can be found in Table 1.

Despite the considerably large sample size, the economic data presents a substantial missing data rate of 71.2 %. Most missing data are concentrated in developing countries, such as countries in Africa (Fig. 1a). Fig. 1b shows a significant negative correlation ($R = -0.622$) between the missing rate and the level of economic development. In the temporal dimension, data were nearly absent after 2014, with an annual missing rate of approximately 65 % from 1992 to 2014 (Fig. 1c). Therefore, only relying on official sub-national statistical data for economic risk assessment was likely to introduce bias, and its reference importance for developing countries was limited.

To verify the MAUP issue in cross-scale predictions, we compared the correlation of economic data compiled by different authors with the sub-national-scale economic data used in this study (Kalkuhl & Wenz, 2020). They include official statistics compiled by Gennaioli et al. (Gennaioli et al., 2013) (Fig. 2a), gridded GDP estimated by Chen et al. (Chen et al., 2022) (Fig. 2b), and gridded GDP estimated by Wang and Sun (Wang & Sun, 2022) (Fig. 2c). All the economic data were transformed into GDP per capita in US dollars using population counts from the LandScan Global Population database (Bhaduri et al., 2007), and were then

Table 1
Data used for developing long term time series economic data.

Datasets	Unit	Spatial resolution	Period	Source
Sub-national GDP per capita	USD	Sub-national (i.e., province, state, etc.; depending on country in question)	1992–2016	Kalkuhl and Wenz (Kalkuhl & Wenz, 2020)
National GDP per capita	USD	National (countries around the world)	1992–2021	World Bank Open Data base(https://data.worldbank.org/)
DMSP	DN	About 1000 m, spanning –180 to 180 degrees longitude and –65 to 75 degrees latitude with WGS-84 projection	1992–2013	NOAA/NGDC (https://www.ngdc.noaa.gov)
VIIRS	nW/cm ² /sr ¹	About 500 m, spanning –180 to 180 degrees longitude and –65 to 75 degrees latitude with WGS-84 projection	2013–2021	NOAA/NGDC (https://www.ngdc.noaa.gov)
Administrative units	–	National and sub-national	Accessed at 1 October 2019	GADM Version 3.6 (https://gadm.org)

Note: GADM represents the Database of Global Administrative Areas. The global NTL data were uniformly resampled to a 1000 m resolution under the WGS-84 projection.

logarithmically scaled. Fig. 2a provides evidence on the reliability of the data used in this study indicated by a high correlation ($R=0.910$ and RMSE=1.071) with the official economic data compiled by Gennaioli et al. However, when scrutinizing the gridded GDP estimated based on national-scale economic data, there was a significant decline in accuracy at the sub-national scale for both datasets. Data estimated by Wang and Sun (Wang & Sun, 2022) showed a more pronounced issue in accuracy. To ensure the robustness of our results, we further employed the population count from WorldPop (Tatem, 2017) to adjust the GDP figures into GDP per capita. The results showed remarkable consistency: $R=0.910$ (Fig. 2a), $R=0.765$ (Fig. 2b), and $R=0.682$ (Fig. 2c). This further emphasized the importance of establishing the relationship between economic activity and NTL at the sub-national scale, if the target is to develop sub-national-scale economic statistics.

3. Methodology

As shown in Fig. 3, our methodology began with the necessary pre-processing of two types of NTL data to eliminate noise in VIIRS and address inconsistencies in DMSP. Then, under the modeling philosophy of spatial statistics, the multi-layer perceptron and Light Gradient Boosting Machine algorithms was developed to integrate the DMSP and VIIRS data. Finally, a novel modeling strategy based on multi-layer perceptron algorithm was developed to establish a conversion relationship between NTL and GDP per capita.

3.1. Primary calibration of VIIRS data and DMSP data

Following the methodologies used by (Chen et al., 2021) and (Liu et al., 2010), and utilizing Google Earth Engine (Xie et al., 2024), we derived annual composite VIIRS data by computing the median value of the monthly data sets for each pixel at each year. To mitigate the impact of stray light pollution during the summer, monthly data from June to August were excluded. Subsequently, to eliminate background noise and extreme values, pixels with values below $1 \text{ nW cm}^{-2} \text{ sr}^{-1}$ were considered as background noise and set to 0 (Chen et al., 2021). To mitigate the impact of extreme outliers, four highly developed cities, that is, New York City in the United States, London in the United Kingdom, and Shanghai and Beijing in China were selected as reference cities to determine the threshold for maximum NTL intensity detection. If the pixel value exceeded the threshold, the maximum value below the threshold within the eight neighboring pixels was considered an alternative value. In line with the invariant region method used by (Elvidge et al., 2009) and (Shi et al., 2016), the power function (Eq. A1) and Japan as an invariant region was used to reduce the saturation effect in DMSP. In consistence with (Shi et al., 2016; Zhang & Seto, 2011), annual continuous processing with a base year of 1992 was conducted (Eq. A2).

3.2. Integration of the long time-series nighttime lights data under the modeling philosophy of spatial statistics

To eliminate inconsistencies between DMSP and VIIRS, we used second-order neighborhood information from VIIRS to expand the DMSP data (Fig. 4a). The underlying assumption of this method is that pixel blurring caused by the blooming effects or spillover effects in DMSP can be reconstructed using neighborhood information from VIIRS, which provides a more accurate representation of nighttime lights.

$$DN(u, v) = f\left(\tilde{x}(u, v), \tilde{N}^2(u, v)\right) + \epsilon, \quad (1)$$

where, $DN(u, v)$ represents the DN value of DMSP at pixel coordinates (u, v) ; $\tilde{x}(u, v)$ represents the logarithmically scaled VIIRS radiance at the corresponding location (Yu et al., 2018); $\tilde{N}^2(u, v)$ represents the second-order neighborhood pixels of VIIRS; and ϵ denotes the model residual

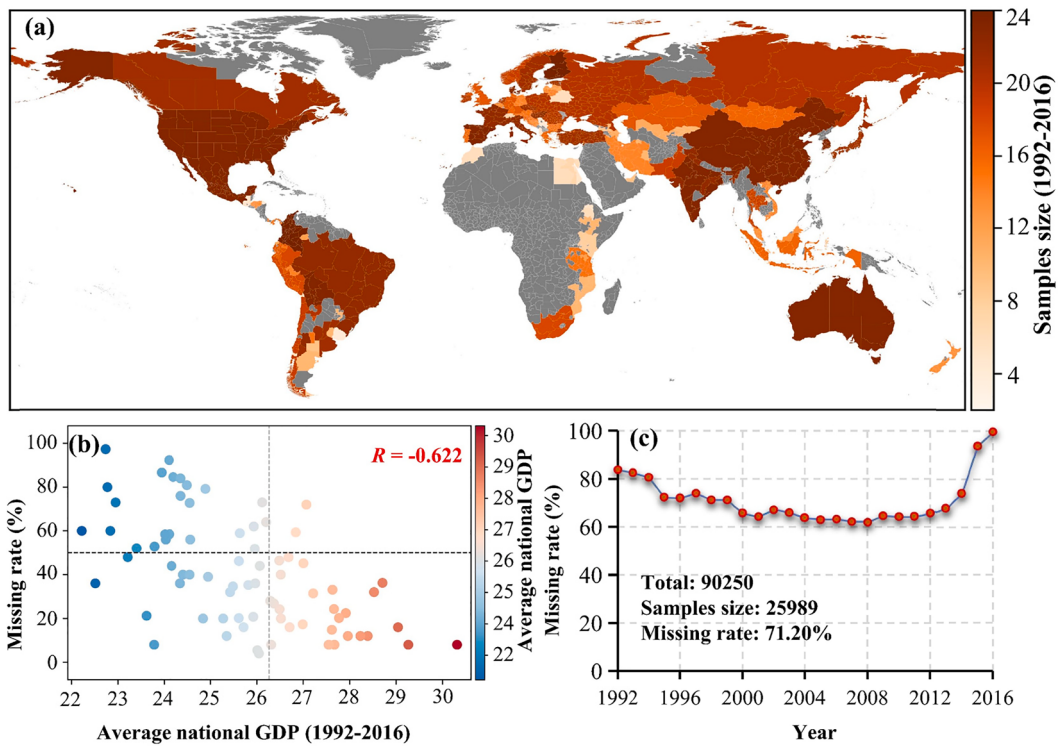


Fig. 1. Missing rates of sub-national official economic data compiled by Kalkuhl and Wenz (Kalkuhl & Wenz, 2020) in time and space. (a) Sample size of sub-national official economic data from 1992 to 2016; (b) Scatter plot of economic development level and missing rate, excluding regions with a 100% missing rate; (c) Missing rate of sub-national official economic data from 1992 to 2016. The missing rate is calculated as one minus the ratio of the actual amount of data to the expected amount of data. The average national GDP, calculated by averaging a nation's GDP series from 1992 to 2016, serves as a representative measure of a nation's economic development level. The symbol R corresponds to the Pearson correlation coefficient. The term "total" refers to counts of all sub-national regions considered during the study period, while "sample size" refers to counts of sub-national regions for which data is available.

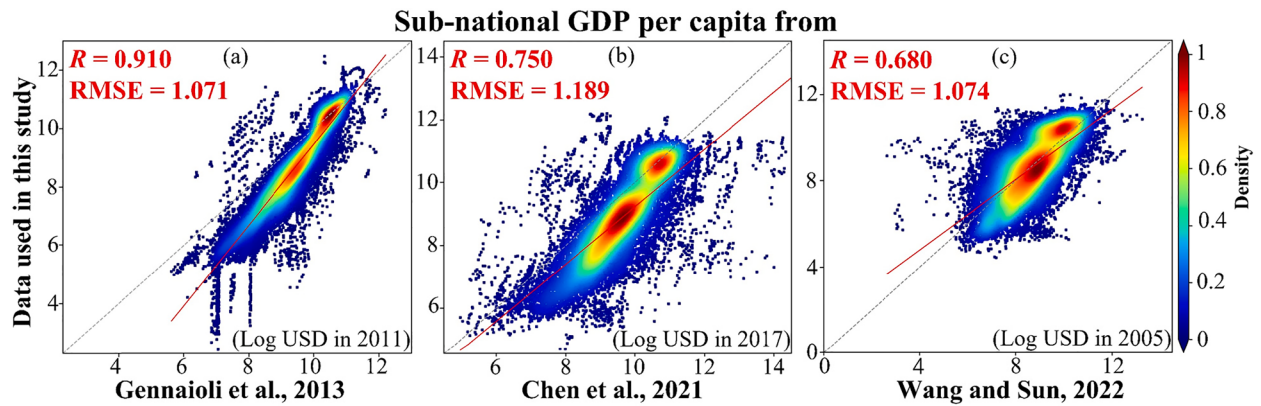


Fig. 2. Comparison of different economic datasets. RMSE represents root-mean-square error. The gridded economy data was aggregated to sub-national scale using administrative unit boundaries.

term. Fig. 4 illustrates the mapping process from the VIIRS to the DMSP. For this mapping, an intuitive solution to imitate the spillover effect is to take the convolutionally transformed VIIRS data as the input variable, using kernel density in (Li et al., 2020), (Wu et al., 2022). Kernel density assumes spatial stability and isotropy, thereby reducing multidimensional neighborhood information to one-dimensional neighborhood information, which may lead to information loss. This study, therefore, constructs eight spatial variables capturing effects of first-order neighbors, and sixteen spatial variables capturing effects of second-order neighbors. The coefficients of these spatial neighborhood variables can be regarded as weights assigned to relevant neighbors from a VIIRS layer. These weights can be estimated by minimizing a loss function, such as the mean squared error

(Eq. (4)).

$$DN(u, v) = a + \beta_0 \tilde{x}(u, v) + \epsilon, \text{ Without neighborhoods}; \quad (2)$$

$$DN(u, v) = a + \beta_0 \tilde{x}(u, v) + \mathcal{W} \tilde{N}^2(u, v) + \epsilon, \text{ With neighborhoods}; \quad (3)$$

$$\text{MSE} = \frac{1}{n} \sum_{i=1}^n (DN(u, v) - \widehat{DN}(u, v))^2, \text{ Lost function}, \quad (4)$$

where, a , β and \mathcal{W} represent the regression parameters estimated using the ordinary least squares method. An intriguing result emerged in our analysis. In a model that does not incorporate neighborhood information

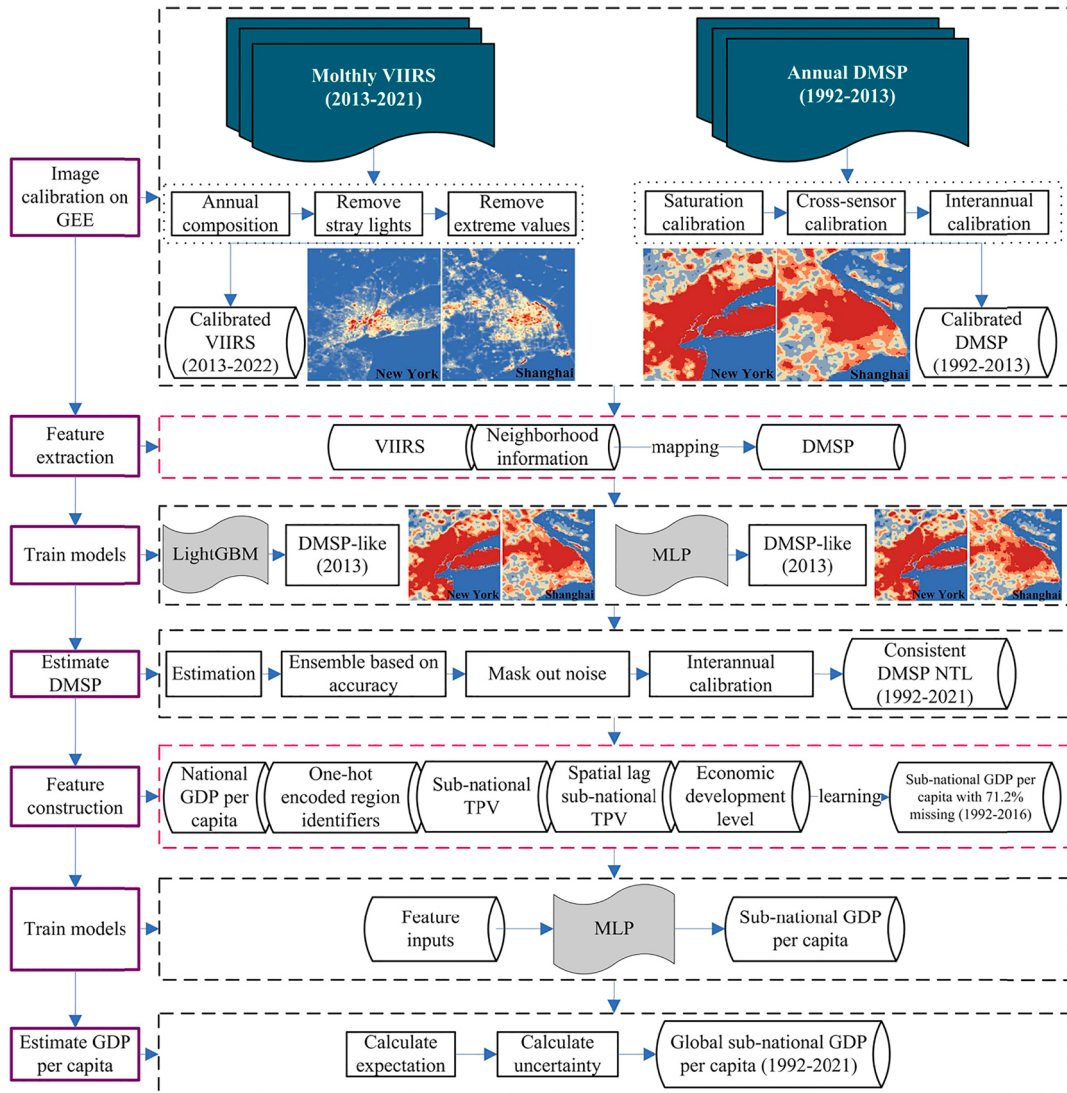


Fig. 3. The flow of methods used in developing the sub-national scale economic data.

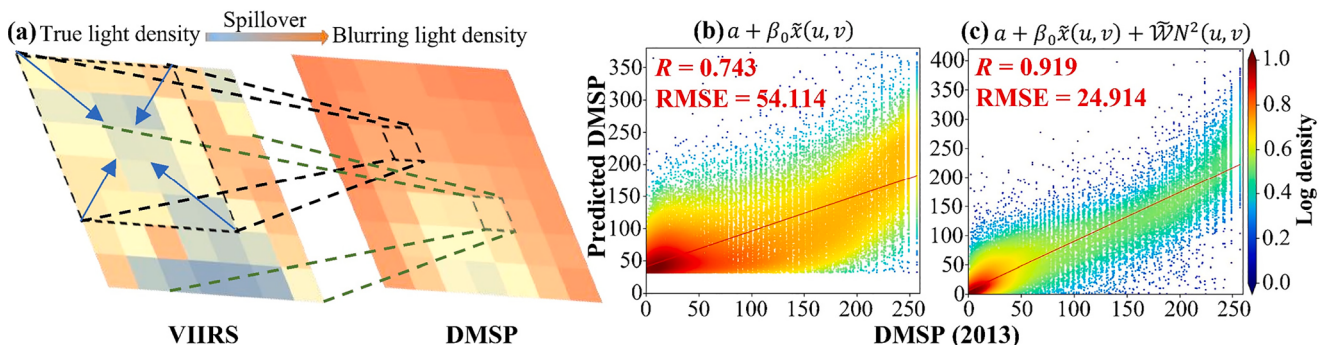


Fig. 4. The mapping between the neighborhood information of VIIRS to DMSP (a); estimation accuracy of the linear model without neighborhood information (b); and estimation accuracy of the linear model exploiting neighborhood information (c).

In Eq. (4), the Pearson correlation coefficient (R) between the estimated and observed values was 0.743, accompanied by a root-mean-square error (RMSE) of 54.114 (Fig. 4b). However, with the inclusion of neighborhood information in Eq. (5), the correlation coefficient is improved significantly to 0.919, accompanied by a reduced RMSE of 24.914 (Fig. 4c). This improvement in accuracy provides evidence supporting the underlying assumptions.

As shown in Fig. 4b and c, a non-linear relationship was observed between DMSP and VIIRS. To capture the nonlinear relationship, we employed two approaches, that is, a deep learning method—a multi-layer perceptron algorithm implemented in the Python package TensorFlow (version 2.12.0) (MLP) and a machine learning method—a gradient boosting decision tree (GBDT) implemented in the Python package LightGBM (version 3.3.5). In our approach (Fig. 5), the multi-

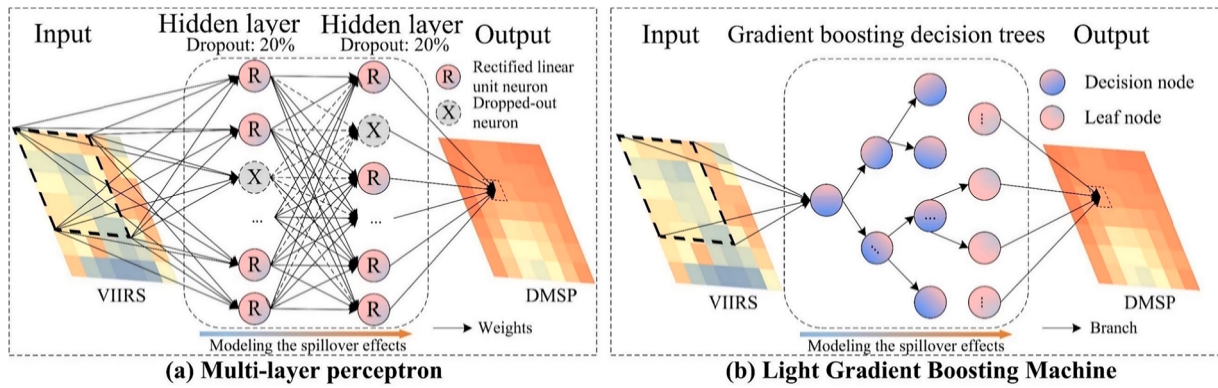


Fig. 5. Modelling the non-linear relationship between VIIRS and DMSP using MLP (a) and LightGBM (b), while taking into account spillover effects.

layer perceptron algorithm is trained using the backpropagation technique and optimized using the Adaptive Moment Estimation (Adam) optimizer. Following the methodologies proposed by (Chen et al., 2020; Li et al., 2020), the latitudes and longitudes of the pixels were incorporated into the models. To mitigate overfitting, dropout layers are introduced in each hidden layer (Srivastava et al., 2014).

rely on data standardization. Therefore, when training the LightGBM, data normalization was intentionally omitted to preserve the integrity of the original data. Considering the heterogeneity among continents, we model the data separately for the six continents: North America, South America, Africa, Oceania, Asia, and Europe. As Antarctica has no available data, it is excluded from analysis. After model training, MLP

$$\begin{aligned} X(u, v) &= (\tilde{x}(u, v), \tilde{N}^2(u, v), u, v), \text{ Input} \\ h^{(1)} &= \sigma(W^{(1)}X + b^{(1)}), \text{ Hidden layer 1 with 200 node and Dropout layer (20\%)} \\ h^{(2)} &= \sigma(W^{(2)}h^{(1)} + b^{(2)}), \text{ Hidden layer 2 with 200 node and Dropout layer (20\%)} \\ DN &= W^{(3)}h^{(2)} + b^{(3)} + \epsilon, \text{ Output,} \end{aligned} \quad (5)$$

where X is the complete input matrix, $h_i^{(l)}$ the output of the hidden layer l in the neural network, $W^{(l)}$ the weight matrix of the neural network, and b is the bias vector.

The LightGBM algorithm, a highly efficient non-linear machine learning algorithm developed by Microsoft Research (Ke et al., 2017), was developed to integrate the DMSP and VIIRS data. LightGBM incorporates Gradient-based One-Side Sampling (GOSS) and Exclusive Feature Bundling (EFB) algorithms to enhance training speed (Su et al., 2021). Compared with traditional GBDT algorithms, LightGBM offers faster training and prediction tasks with a smaller memory footprint without sacrificing accuracy. The gradient boosting decision trees, also optimized by minimizing the mean squared error (MSE), are constructed as follows.

$$DN = \sum_{k=1}^K f_k(X), f_k \in \mathcal{F}, \quad (6)$$

where \mathcal{F} represents the function space of the regression forest and f_k represents the weights of the leaf nodes where the samples are assigned in the k -th tree. The hyperparameters of the LightGBM were carefully tuned using the grid search method to ensure optimal performance.

Two model are trained by minimizing the mean squared error (MSE) loss function. Prior to training the model, samples from the overlapping year of 2013 were partitioned into a training set (55 %), a validation set (25 %), and a test set (20 %). And an early stop strategy was adopted to prevent overfitting of the model (Srivastava et al., 2014). To mitigate the influence of unit differences, min-max normalization was applied to both input and output factors. As an ensemble learning algorithm, the LightGBM is inherently robust to variations in data units and does not

and LightGBM were used to estimate DMSP-like data from 2014 to 2021. For calibration purposes, the 2013 DMSP data served as a mask to identify non-zero pixels in the DMSP-like estimation. Given that MLP and LightGBM could offer different yet complementary strengths, ensemble is used to leverage the strengths of two approaches: the estimations from the deep and machine learning models are further weighted based on their relative accuracies, producing a more robust DMSP-like dataset (DN_{robust}).

$$DN_{robust} = \frac{R_{MLP}^2 DN_{MLP} + R_{LightGBM}^2 DN_{LightGBM}}{R_{MLP}^2 + R_{LightGBM}^2}, \quad (7)$$

where, R_{MLP}^2 and $R_{LightGBM}^2$ are squared model estimation accuracy from MLP and LightGBM, respectively; $DN_{LightGBM}$ and DN_{MLP} are model estimations of MLP and LightGBM, respectively.

Table 2
Hyperparameter tuning strategy in MLP and LightGBM.

MLP Hyperparameters	Parameter range	LightGBM Hyperparameters	Parameter range
Optimizer	adam, sgd, rmsprop	Objective	regression_l1, regression_l2, poisson
Activation Function	relu, tanh	Max depth	20, 30, 40, 50
Learning rate	0.01, 0.001	Number of leaves	20, 40, 60, 80
Number of neurons in layer 1	100, 200, 300	Minimum number of subsamples	18, 19, 20, 21, 22
Number of neurons in layer 2	100, 200, 300	Learning rate	0.01, 0.001
Dropout rate	0.1, 0.2, 0.3	Subsample	0.8, 0.9
Total parameter combination	324	Total parameter combination	960

The training process of MLP and LightGBM involved a comprehensive evaluation of numerous hyperparameters. Optimal settings were determined using a grid search methodology that considers prediction accuracy, generalization ability, and computational cost as key metrics. Given the large sample size of the global dataset and numerous hyperparameter combinations, to manage computational burden, a 1% random sample was drawn for each continent, yielding approximately 100,000 samples. For both MLP and LightGBM, only hyperparameters that may significantly influence model outcomes are selected for tuning. The specific ranges of these parameters are reported in Table 2. For the MLP, hyperparameter combinations consistently achieving a prediction accuracy above 0.94 included the Adam optimizer, a learning rate of 0.001, and the ReLU activation function. Variations in the number of neurons and dropout rate had a much smaller impact on prediction accuracy, affecting it by an order of magnitude of 0.001 and MSE by 0.0001. To balance training time and generalization capacity, the configuration was set to 200 neurons per layer with a dropout rate of 20%. Results from LightGBM indicated that hyperparameter combinations with a prediction accuracy exceeding 0.95 were associated with the “regression l2” and “poisson” objectives. The median training times for these objectives were 13.2 s and 43.2 s, respectively, with corresponding median prediction accuracies of 0.9503 and 0.9507. Consequently, the “regression l2” objective was selected. Further adjustments in parameters showed marginal differences in prediction accuracy (0.001 order of magnitude) and MSE (0.0001 order of magnitude). To balance training time and generalization capacity, settings of max depth (40), number of leaves (80), subsample (0.9), minimum number of subsamples (20), and learning rate (0.01) were adopted.

3.3. Construct the relationship between GDP per capita and NTL

After compiling a long-term time series of NTL data had been obtained, this study developed a novel modeling strategy based on the MLP to establish the dynamic relationship between NTL and GDP per capita at the sub-national scale. *It was hypothesized that sub-national economic growth trends fluctuated around the national economic growth trend, with the extent of fluctuations captured by variations in the intensity of sub-national NTL* (Fig. 6). Consequently, the national scale GDP per capita and total pixel values (TPV) of NTL at the sub-national scale were selected as the primary input data. Considering the spatial clustering effect inherent in economic development, the model incorporated a spatial lag term for TPV at the sub-national scale. To account for regional heterogeneity, sub-national regional identifiers were encoded using a one-hot encoding scheme and were included in the model (Thorsen-Meyer et al., 2022). *Doing this also allows the hierarchical data structure where sub-national units nest into countries to be modeled*. Given the relatively small sample size of the modeled sub-national GDP per capita, a neural network with fewer nodes was selected as the model architecture (Eq. (8)), and the Adam optimizer was used.

$$\begin{aligned} X_r &= (E_c, DN_r, \text{lag}(DN_r), E_l, \text{oneHot}(ID)) \text{ Input} \\ h^{(1)} &= \sigma(W^{(1)}X_r + b^{(1)}) \text{ Hidden layer 1 with 10 nodes.} \\ h^{(2)} &= \sigma(W^{(2)}h^{(1)} + b^{(2)}) \text{ Hidden layer 2 with 10 nodes.} \\ E_r &= W^{(3)}h^{(2)} + b^{(3)} + \epsilon \text{ Output,} \end{aligned} \quad (8)$$

where, DN_r represents the TPV of a sub-national region or unit. $\text{lag}(DN_r)$ denotes the spatial lag of DN_r , calculated using a spatial adjacency weight matrix. E_c refers to national-scale GDP per capita, E_l refers to the economic development level and $\text{oneHot}(ID)$ represents the one-hot encoding of regional identifiers. $W^{(l)}$ refers to the weight matrix of the neural network and b represents the bias vector.

To further consider potential heterogeneity in the relationship between NTL and GDP across varying development stages, we divided countries into 10 categories based on their average national-scale GDP per capita from 1992 to 2021, using a natural break-point method (Fig. 7). These groupings acted as control variables for economic development stages. Before training the model, the samples were randomly divided into training (50%), validation (20%), and testing (30%) sets. The test set remained independent of the training and validation sets, and was not involved in any model training process. This setup allowed us to simulate missing data in both temporal and spatial dimensions. Upon meeting the predefined training stop criteria, the trained model is employed to predict the GDP per capita, a procedure referred to here as one training cycle.

To account for potential impacts of sampling uncertainty on model estimation, we conducted 100 cycles of model training and prediction. In each cycle, samples were randomly divided into training, validation, and test sets as mentioned above. Then, for each sub-national region, we calculated the variance and mean of predictions to assess uncertainty of model results.

4. Results and discussion

4.1. Evaluating the DMSP-like data

4.1.1. Evaluate the global accuracy of DMSP-like data

The accuracy of the test set, independent of the training and validation sets, was used as an evaluation metric for the models. As depicted in Fig. 8 and Table A1, all Pearson correlation coefficients exceeds 0.95 and a regression slope close to one, indicating high accuracy of the reconstructed nonlinear relationship between VIIRS and DMSP. The accuracies for the training and test sets exhibit negligible differences (Table A1) from the accuracy for the test set, indicating absence of overfitting in the trained models.

We then compare the DMSP data estimated here with previous data products from recent studies that are dedicated to produce long time-series of nighttime lights at the global scale. For ease of exposition, we denote the developed DMSP-like data from Li et al. (2020) (Li et al., 2020) as “Li”, and data from Nechaev et al. (2021) (Nechaev et al., 2021) as “Nechaev”. Globally, the resemblance of our DMSP-like data with Li

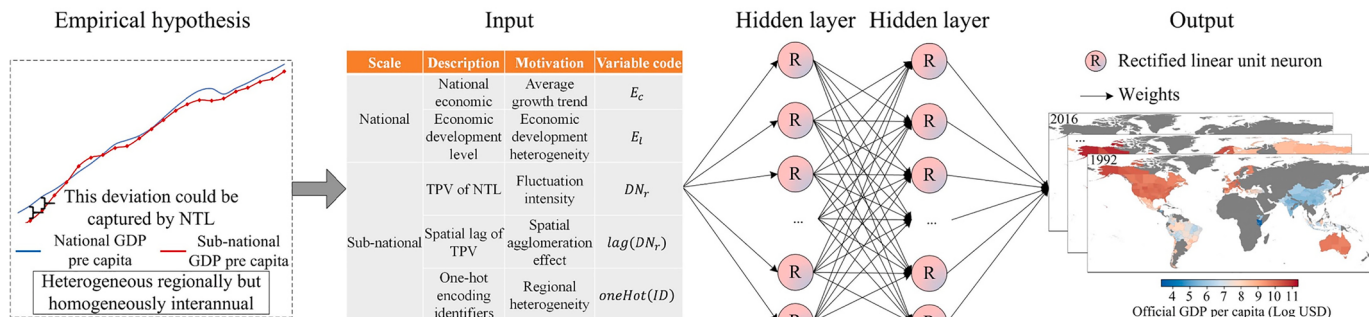


Fig. 6. The conceptual framework for modeling the relationship between NTL and the economy.

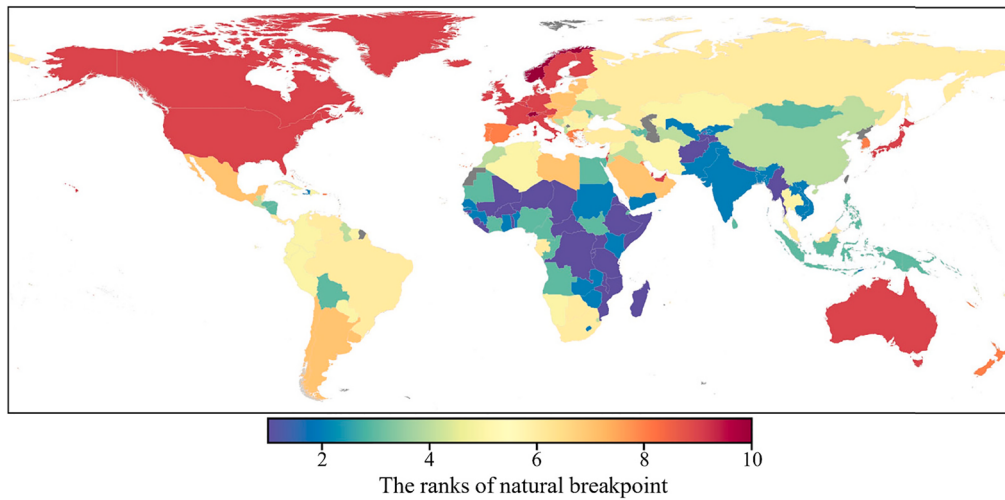


Fig. 7. Countries at various economic development stages.

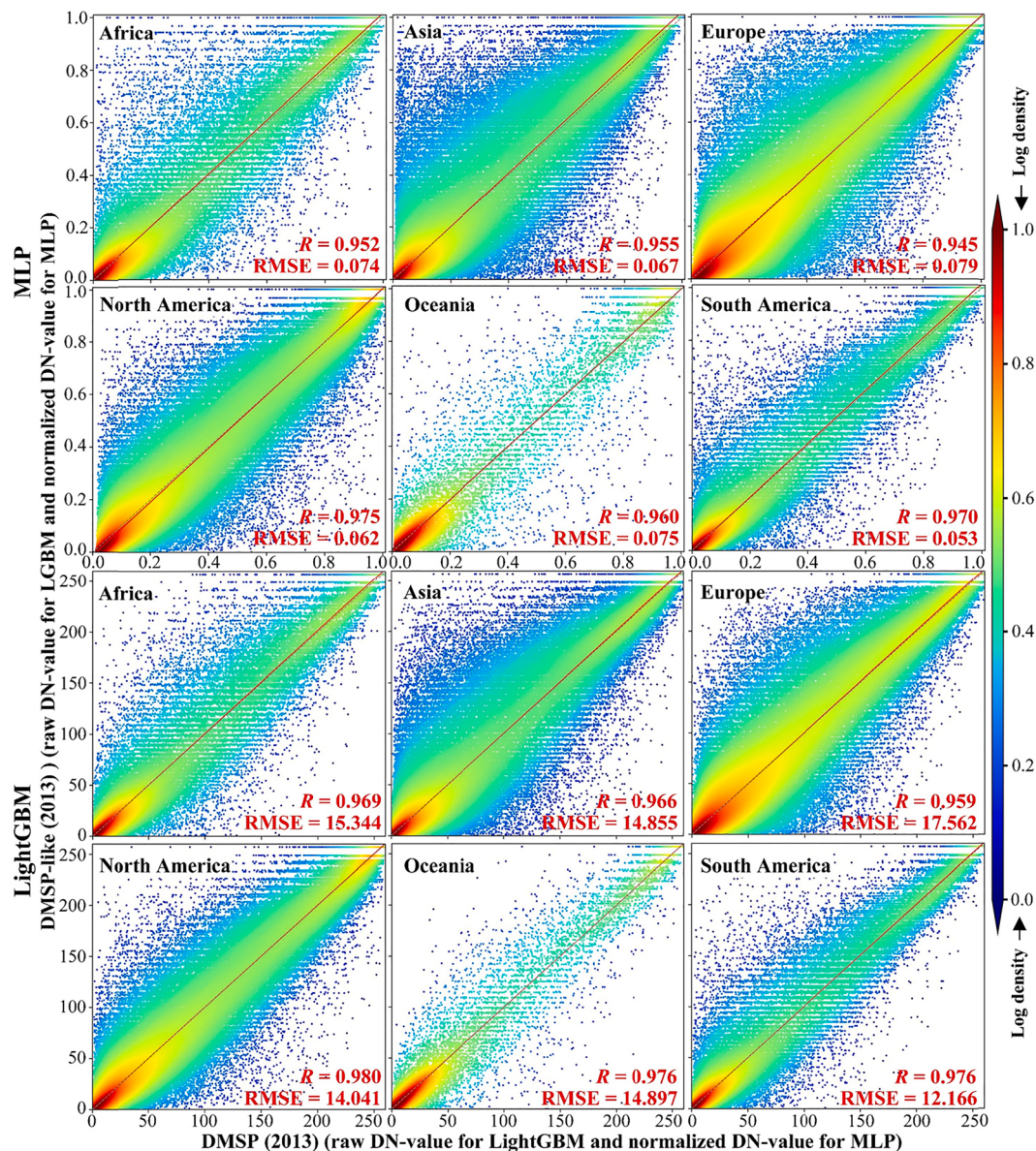


Fig. 8. Scatter density plot of observed and estimated values for the test set pixels.

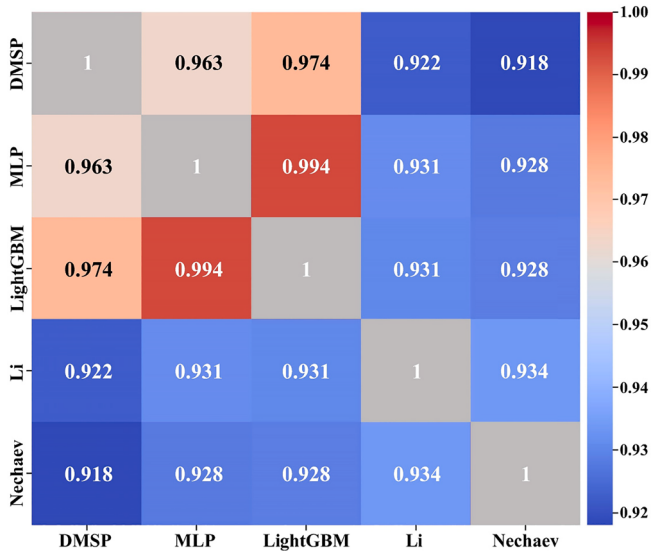


Fig. 9. Correlation coefficient matrix of different DMSP data.

and Nechaev is high, with Pearson correlation coefficients being roughly 0.93 for year 2013 (Fig. 9). The correlation between our DMSP-like data with Li and Nechaev remains high and consistent across year after 2013, with all Pearson correlation coefficients being above 0.92. It is useful to note that the MLP and LightGBM models yield out-of-sample accuracy of 0.963 and 0.974, respectively. These figures are comparable to the

accuracy of 0.97 from [45], achieved by using a complex Residual U-Net deep learning model (Nechaev et al., 2021). Additionally, both MLP and LightGBM models reduce model complexity and facilitates faster training (less than two hours for MLP and 30 min for LightGBM), which can be important for studies on bootstrapping- or permutation-based uncertainty quantification of DMSP-like nighttime lights data product.

4.1.2. Evaluate the local accuracy of DMSP-like data

Further evaluation on local accuracy of the compiled data is performed, focusing on New York, London, Beijing and Shanghai in Asia, and Nile Delta and Harare in Africa (Fig. 10). The DMSP-like data estimated by both MLP and LightGBM exhibits close resemblance to the original DMSP data in terms of spatial extent and features. The high-value ranges of the DMSP-like data closely align with the corresponding satellite imagery from Google Earth, whereas the VIIRS data predominantly capture areas with high nighttime lights intensity such as city centers. In addition, we assess lights variability along a specific geographical transect that captures the spatial configuration of a city, as shown in Fig. 10. The profile characteristics revealed by our DMSP-like data exhibit a notable consistency with those observed from the original DMSP data, thereby validating the reliability of our conversion process from VIIRS to DMSP. Local variabilities do exist, for instance, our DMSP-like data closely mirror Li's data for New York, London, and Beijing, while it aligns well with Nechaev's data for Shanghai and the Nile Delta region. Such localized divergence in profile characteristics potentially suggest that different methodologies may offer distinct advantages in modeling localized nuances of nighttime lights. Correlation and distribution analysis depicting nighttime lights corresponding to these data

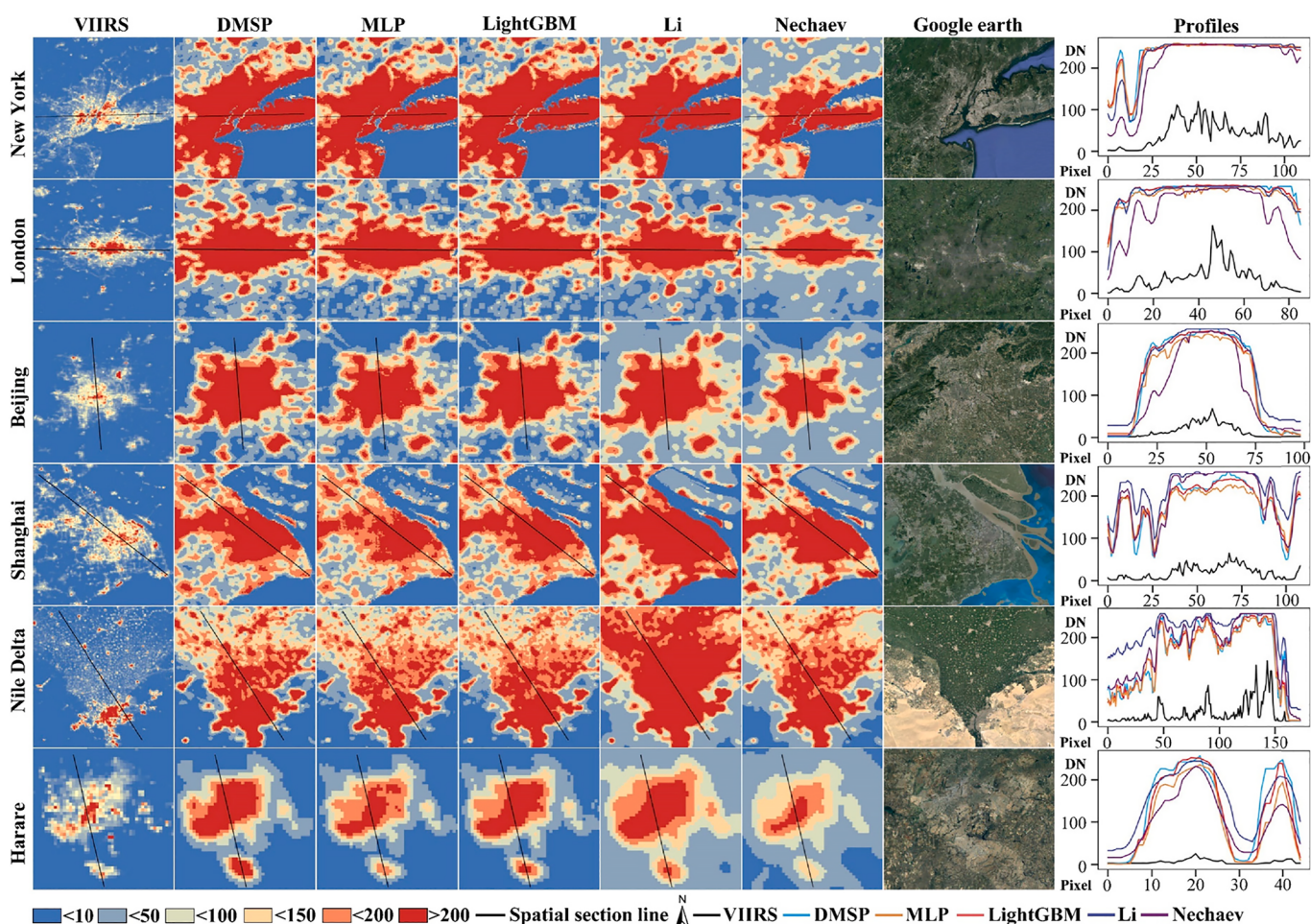


Fig. 10. Profile patterns of nighttime illumination revealed by DMSP, DMSP-like, and VIIRS data for New York, London, Beijing, Shanghai, Nile Delta, and Harare.

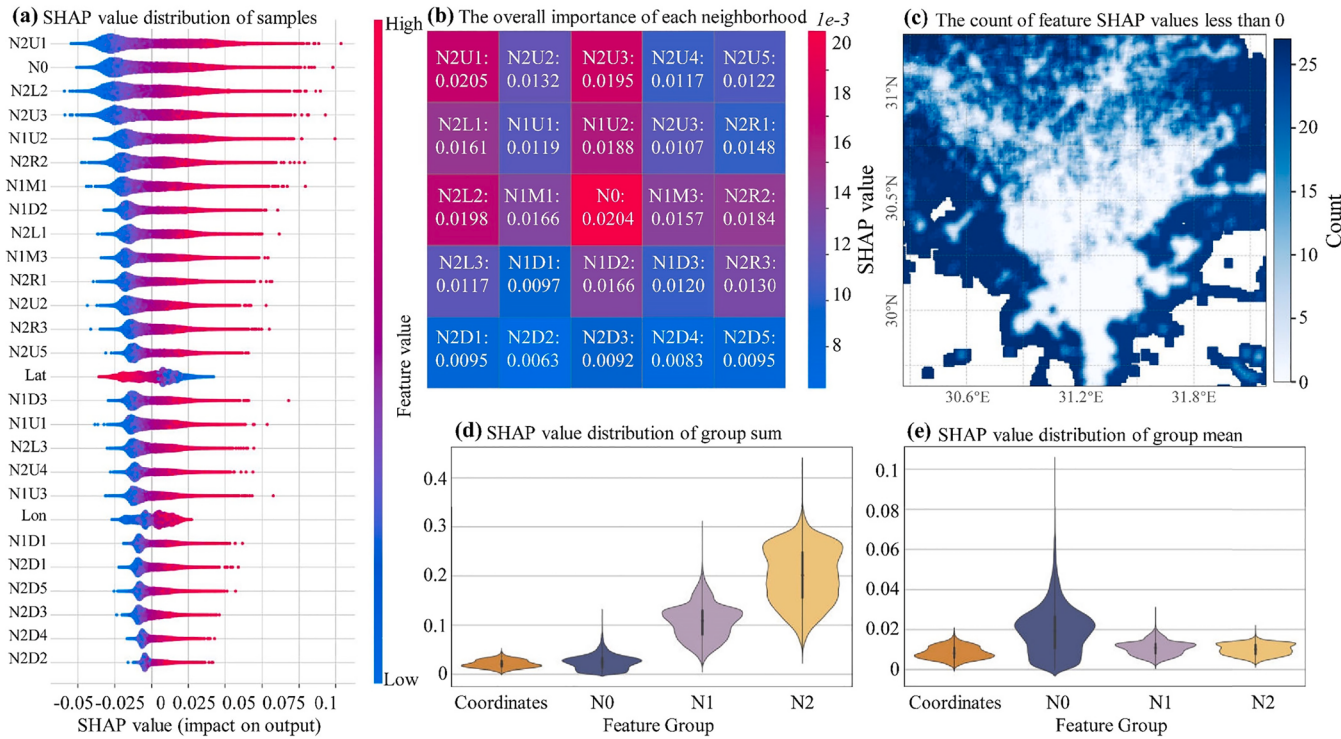


Fig. 11. Feature importance analysis results from the MLP model. Note: N0 denotes the focal pixel, N1 denotes the first-order neighborhood, and N2 denotes the second-order neighborhood. The symbols “U”, “D”, “L”, and “R” indicate pixels situated above, below, to the left, and to the right of the focal pixel, respectively. For instance, the code “N2U3” refers to the third second-order neighbor located above the focal pixel (N0).

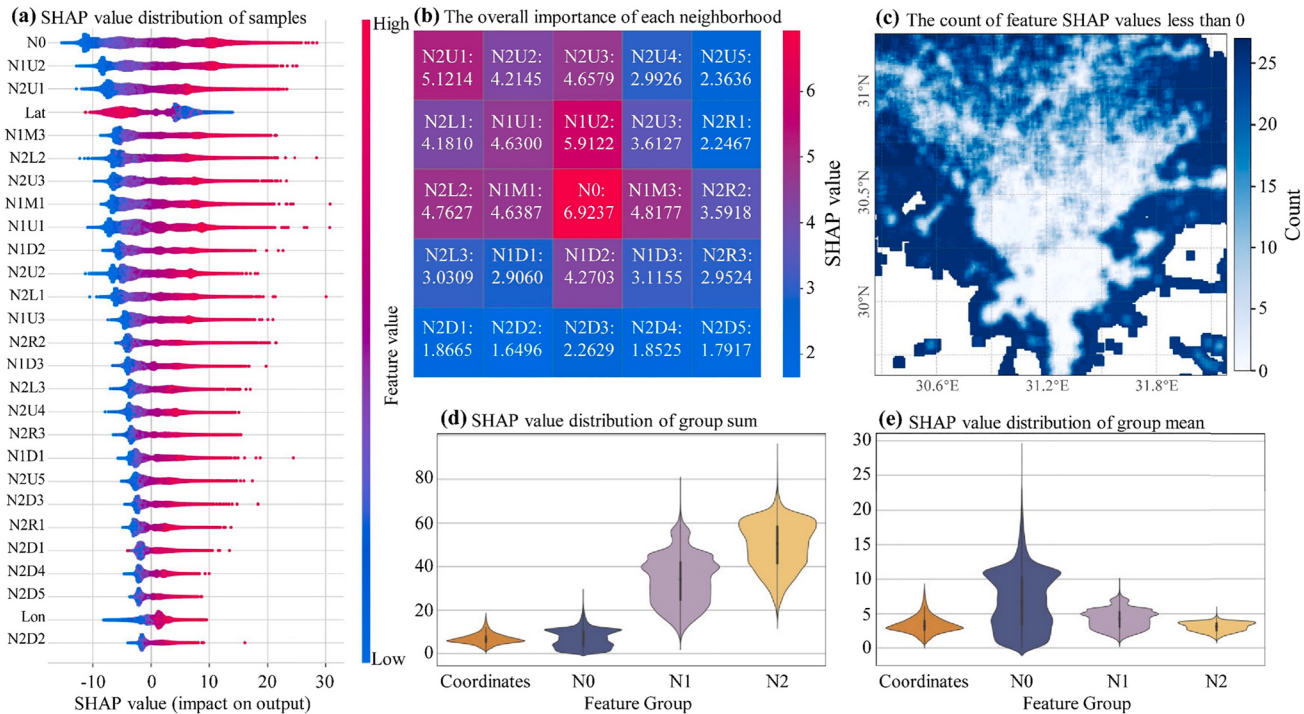


Fig. 12. Feature importance analysis results from the LightGBM model.

and regions can be found in Fig. A1.

4.1.3. Feature importance analysis

SHAP (SHapley Additive exPlanations), as outlined by Lundberg and Lee, provides a unified framework for interpreting machine learning

model predictions and analyzing marginal contributions of features to prediction outcomes (Lundberg & Lee, 2017; Zhang et al., 2023). Here, we leverage SHAP to assess feature importance within MLP and LightGBM models across six continents, aiming to identify key factors driving prediction accuracies. To manage computational burden, sample

regions were selected for detailed analysis, consistent with those regions depicted in Fig. 10. The selection of regions helps to illustrate regional variability in feature importance. Due to space limitations, Figs. 11 and 12 specifically present the feature importance results from MLP and LightGBM for the Nile Delta, while results for other regions are provided in Figs A2-A11 of the Supplementary Material.

From the MLP results, Fig. 11a presents the distribution of SHAP values, indicating a positive correlation between VIIRS and DMSP lighting values (direct pixels, first- and second-order neighborhoods). Conversely, horizontal and vertical coordinates correlate both negatively and positively, reflecting the latitudinal and longitudinal variations in light intensity in the Nile Delta. Further analysis aggregates the absolute SHAP values of each feature to obtain overall feature importance (Fig. 11b), highlighting that the importance of neighboring pixels often matches or exceeds that of direct pixels, particularly in the northwest direction. Fig. 11d shows that the first- and second-order neighborhoods contribute substantially to the prediction outcomes. When considering the number of features taken into account, the role of NO is elevated (Fig. 11e). Additionally, Fig. 11c, depicting the number of features with negative SHAP values for each sample, shows a clear negative correlation with nighttime lights intensity: higher light intensities correlate with fewer negative SHAP values and vice versa. This suggests that neighboring information crucially enhances prediction accuracy through a balance of positive and negative contributions. Although the rankings of feature importance from LightGBM slightly differ from that obtained from MLP, the key characteristics of feature importance and their aggregated summaries are consistent across the two models.

4.2. Evaluation of the long-term time series economic data

4.2.1. Evaluation of model accuracy

Summaries of model accuracy based on 100 random simulations are shown in Fig. 13. The average accuracies of the training, validation, and test sets are 0.967, 0.959, and 0.959, respectively. The marginal decrease in accuracy (-0.008) from the training set to the testing set indicates that the model exhibited good generalization performance. The expectation of GDP per capita is obtained by averaging the predictions from 100 random simulations. The overall accuracy was 0.967, and RMSE was 0.412, demonstrating that the model effectively captured the nonlinear relationship between NTL and economic development.

As shown in Fig. 14a, the logarithmically scaled GDP per capita exhibited a mixed Gaussian distribution. This may be attributed to the varying characteristics of sub-national regions with different income levels (low, middle, and high), which is in line with the bimodal distribution of GDP often observed in economic studies (Henderson et al., 2012). In addition, the level of uncertainty was relatively low, with a median value of 0.077. Data points outside the interquartile range merely account for 1.082 % of the data, and the maximum uncertainty is less than 0.498 (Fig. 14b). This suggests that the compiled GDP per capita data is not sensitive to sample selection. The spatial distributions

of GDP per capita and associated uncertainties over years are illustrated in Fig. A2.

4.2.2. Evaluation of long-term trends and within-country heterogeneity

One of the primary reasons for the development of sub-national-scale data is the prevalence of missing data, particularly for units in developing countries. These missing data pose challenges to a robust assessment of sub-national economic risks associated with climate change (Otto et al., 2015). This study makes an important contribution in addressing this issue by reducing the missing data rate from 71.2 % to 7.5 %, allowing for an extended time-series analysis (Fig. 15). When compared with the data on sub-national economic output (DOSE) compiled by Wenz et al. (Wenz et al., 2023), despite DOSE presenting a longer time span (1960–2020), it covers only 1,661 sub-national units across 83 countries, which presents a significantly smaller dataset than ours that covers 3462 sub-national regions across 204 countries. The DOSE data (version 2) compiled by Wenz et al (Wenz et al., 2023) is an update of the Kalkuhl and Wenz data (Kalkuhl & Wenz, 2020), by extending the temporary coverage of GDP per capita to year 2020. Therefore, data from 2016 onwards in DOSE serves as a useful out-of-sample verification dataset. We find a high correlation coefficient of 0.953 between the estimated GDP per capita and the updated official statistics during the period of 2016–2020, providing alternative evidence on the accuracy of our estimated economic data. The web link to the code files for this study and the developed economic data was available at: <https://doi.org/10.6084/m9.figshare.24024597>.

Next, to ensure that the estimated economic data effectively capture authentic economic growth patterns and accurately depict the internal variations within countries from 1992 to 2021, further evaluations were implemented at the global, national, and sub-national scales.

At the global scale, our estimated data demonstrated a closer alignment with the actual economic growth patterns when compared to official statistics data, which had a substantial proportion of missing data. This was evident in the economic downturns following the Asian financial crisis (AFC) and global financial crisis (GFC), for which our estimated data capture this economic decline feature properly (Fig. 16). It is useful to note that the global mean of GDP per capita is downward adjusted when taking into account regions with incomplete official statistics that are usually less developed. Overall, the compiled GDP data reflects the pattern of economic growth dynamics that are often observed in economic studies (Henderson et al., 2012). The red line in Fig. 16 represents the variance in GDP per capita at the sub-national scale. This sustained decrease may be due to rapid economic growth of developing countries.

At the national scale, standard deviations of GDP per capita within each country are calculated, which serve as an indicator of internal economic disparities. As shown in Fig. 17, more developed nations tend to exhibit greater internal variation, indicating pronounced within-country economic disparities. In contrast, developing nations, particularly those in the Global South and African, exhibit lower levels of internal disparities. Notably, a temporal trend towards increasing internal

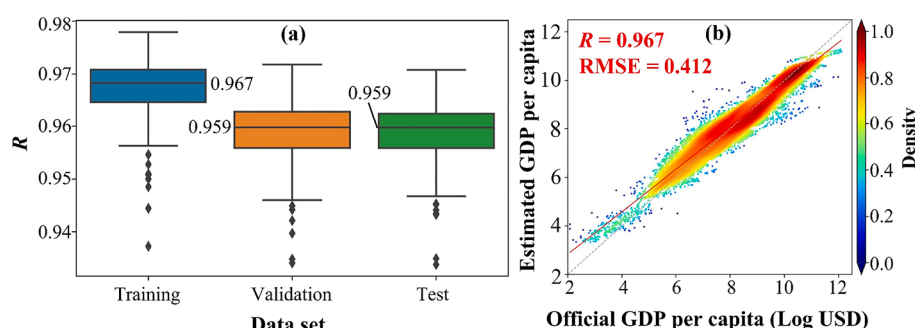


Fig. 13. Training set, validation set, testing set (a), and overall accuracy (b).

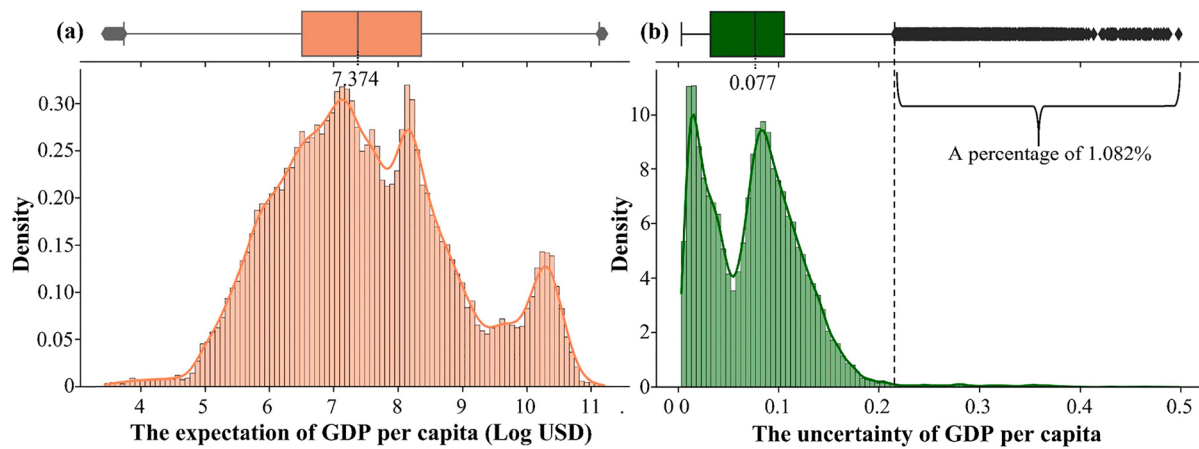


Fig. 14. The distribution of expectation (a) and uncertainty (b) of GDP per capita.

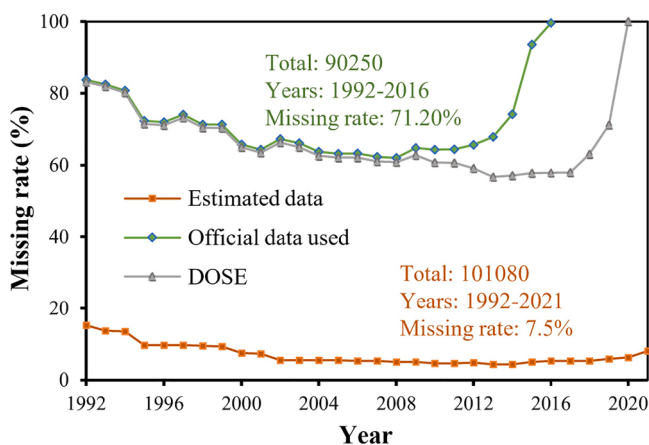


Fig. 15. Percentages of missing data in estimated versus official statistics data.

economic disparity is evident in Fig. 17, empirically substantiating the hypothesis that economic growth tends to amplify regional inequalities (Giannetti, 2002; Kuznets, 1955).

Fig. 18 presents the results of regressing GDP per capita against time at the sub-national scale, calculating growth rates and associated statistical significance for each spatial unit. The rectangular box highlights regions with statistically insignificant growth coefficients, indicative of marked economic volatility in these regions. Moreover, R-squared values from these regression models not only gauge the accuracy of

growth coefficients but also, to some extent, signify economic development instability. Aligning with previous findings, rapid economic growth is predominately observed in developing regions, especially in East Asia with China as a notable example, whereas North America, Australia, and Europe exhibit slower growth (Fig. 18a). Further, to assess the data's reliability in characterizing economic growth trends, we include politically unstable regions in Africa and the Middle East, where official statistics are often sparse.

- 1) For Syria (SYR), the analysis reveals that its sub-national regions exhibit statistically insignificant growth coefficients, coupled with relatively low R-squared values. This trend is likely a consequence of outbreak of the Syrian War in 2011, which precipitated a widespread and rapid economic downturn across various regions.
- 2) Given the absence of national scale economic data for Afghanistan (AFG), the estimated data spans from 2002 to 2021. Fig. 18 illustrates divergent economic growth rates across different regions of Afghanistan. Notably, higher economic growth rates are observed in eastern regions, such as Wardak and Kapisa, whereas southwestern regions, such as Daykundi and Hirat, exhibit slower growth and lower R-squared values. These disparities are largely attributable to the protracted conflict and political instability that have afflicted Afghanistan since 2001.
- 3) While Zimbabwe (ZWE) has not experienced significant political upheaval, the implementation of “Fast Track Land Reform Program” in Zimbabwe in 2000 has led to a gradual deterioration of the economy. Consequently, different sub-national regions within the country have experienced varying degrees of economic decline.

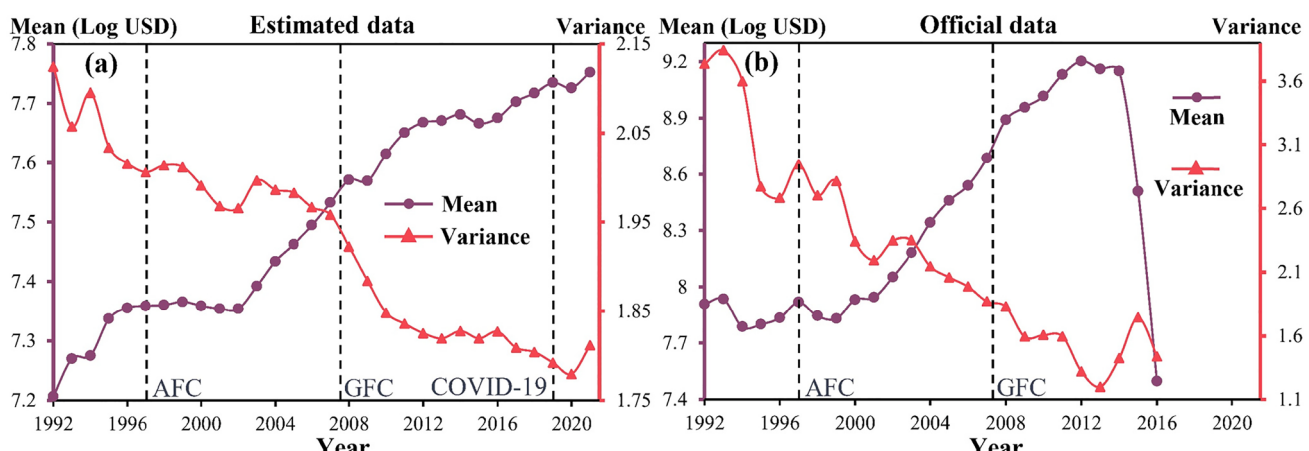


Fig. 16. Average economic growth trends (a) and variances (b) at the global scale calculated from the estimated economic data and official statistics.

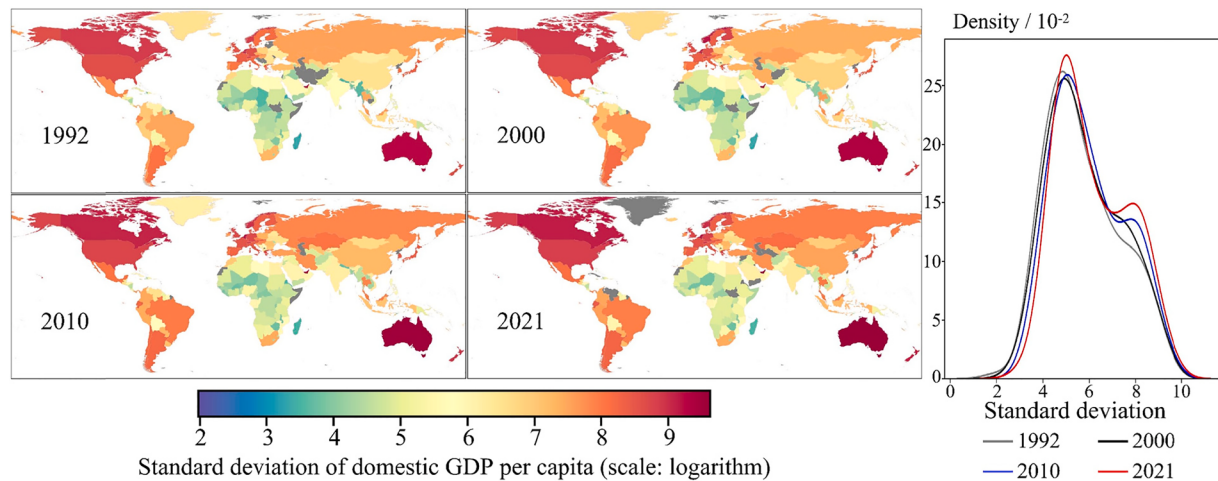


Fig. 17. The standard deviation of GDP per capita within each country.

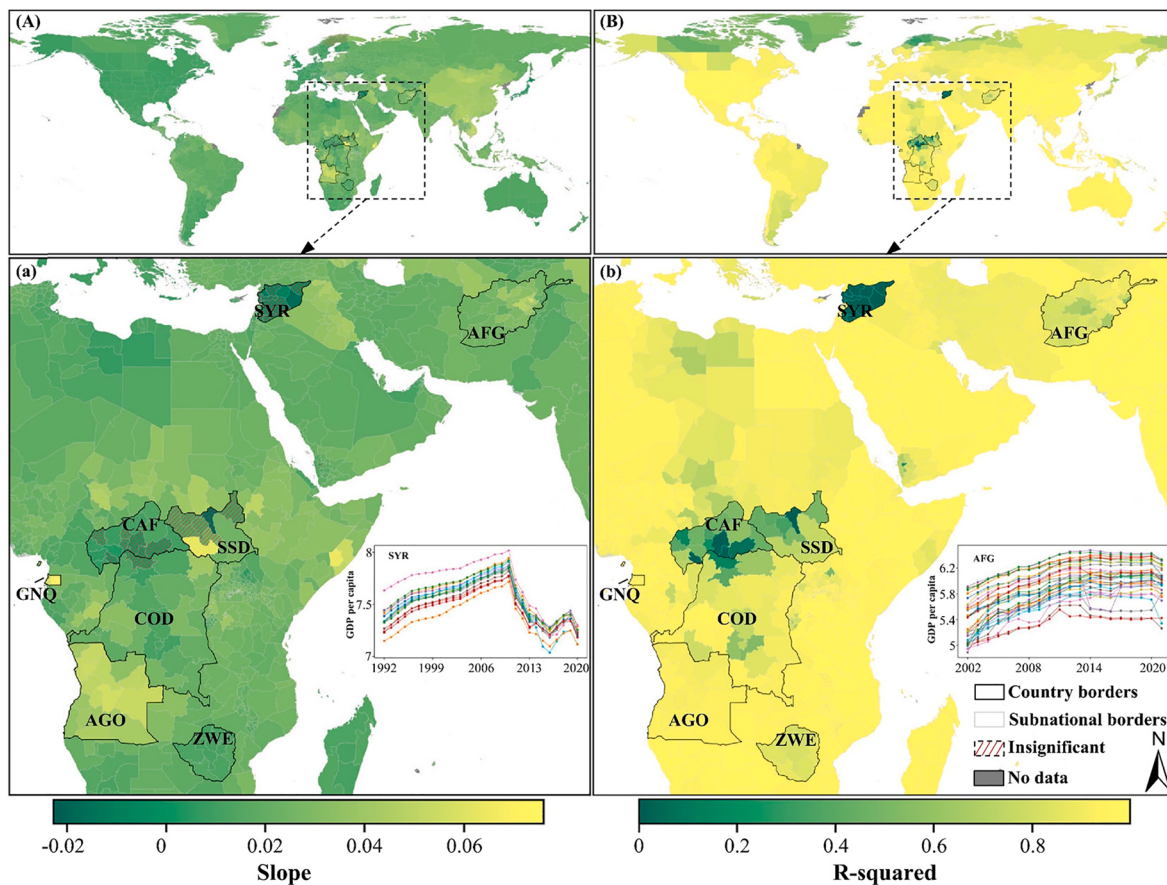


Fig. 18. Regression coefficients (A) and R-squared values (B) from the regression models at the sub-national scale.

- 4) The rapid economic development observed in Equatorial Guinea (GNQ) and Angola (AGO) can be attributed to a confluence of factors: notably, a relatively stable political environment and vigorous oil sector growth have been pivotal in driving this progress.

Finally, the frequency of negative economic growth is quantified, shedding lights on global economic disparities. As demonstrated in Fig. 19, sub-national regions exhibit varying incidences of economic contraction, with more frequent occurrences observed in Africa and high-latitude nations (Fig. 19). Although transient negative growth does

not definitely predict long-term economic trajectories, it often reflects significant fluctuations in economic progress, potentially driven by factors such as extreme weather events and political instability (Carmignani, 2003; Kunkel et al., 1999). The availability of reliable sub-national scale economic growth data, capturing internal variations, is essential for a more accurate and robust assessment of economic risks. This data is particularly vital for refining the precision of projected future economic growth trajectories in the context of a changing climate.

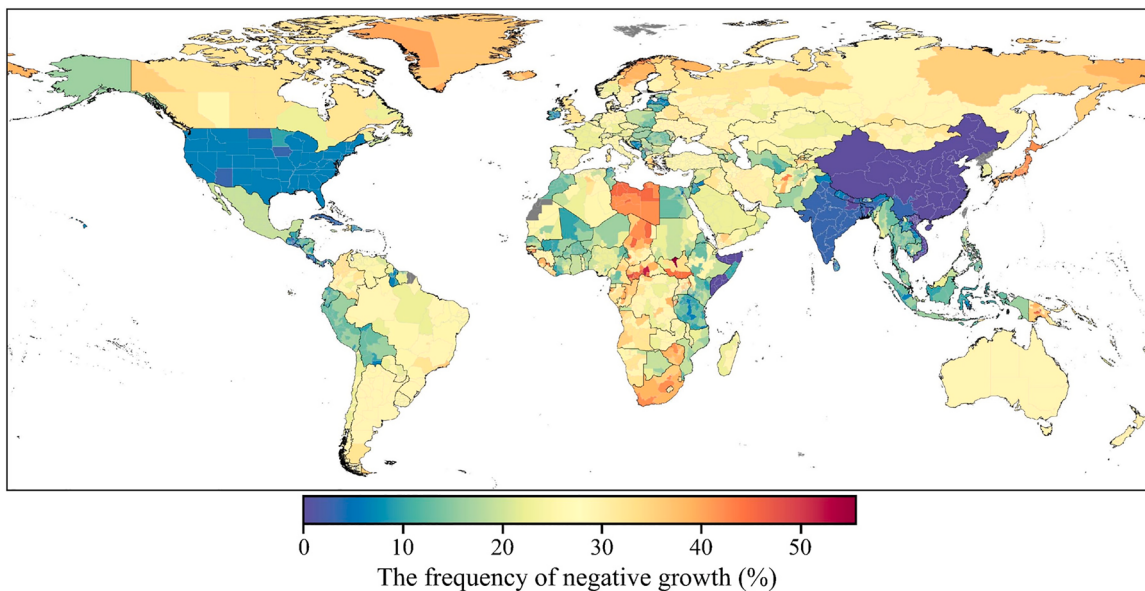


Fig. 19. The frequency of negative economic growth at the sub-national scale.

4.2.3. Using estimated GDP data to assess the impact of extreme heat on global economic growth

We employ a state-of-the-art climate econometrics model (Hsiang, 2016; Kotz et al., 2021) to quantify global economic losses attributed to extreme heat, demonstrating the utility of the estimated GDP data in climate change impact analysis. To assess historical climatic factors, we utilize the fifth generation of the European Centre for Medium-Range Weather Forecasts reanalysis data (ERA5), which offers global hourly updates on temperature (2 m) and precipitation with a spatial resolution of $0.25^\circ \times 0.25^\circ$ since 1940 (Bell et al., 2021). In accordance with the IPCC guidelines (IPCC, 2023), we calculated the intensity of extreme heat, annual mean temperature, total annual precipitation, and temperature fluctuations from 1993 to 2021. These climatic variables were aggregated to the sub-national scale using a population-weighted approach (Kotz et al., 2021), with detailed calculation methodologies presented in Table A2 of the Supplementary Material.

The climate econometrics model is specified as follows:

$$g_{it} = \alpha + \beta_1 T_{xit} + \beta_2 T_{xit} * \bar{T}_{it} + \gamma_1 \bar{T}_{it} + \gamma_2 \tilde{T}_{it} + \gamma_3 P_{it} + \gamma_4 P_{it}^2 + \mu_i + \theta_t + \varepsilon_{it} \quad (9)$$

where g_{it} represents the economic growth rate of region i at year t , T_x denotes the annual extreme heat intensity, \bar{T} the annual mean temperature, \tilde{T} denotes annual temperature variability, P denotes the annual total precipitation, and parameters $[\alpha, \beta, \gamma]$ are the corresponding regression coefficients to estimate. μ_i captures the regional fixed effects to isolate the influence of time-invariant spatial factors on economic and climate variables, and θ_t , a set of year fixed effects, controls for the interannual trends in economic growth and climatic factors. The inclusion of both regional and time fixed effects facilitates causal inferences on the impacts of climate change on economic growth (Wooldridge, 2010; Hsiang, 2016; Kotz et al., 2021). In this illustrative case study, we focus on the impacts of extreme heat (T_x) on economic growth.

Fig. 20 presents the marginal effect of extreme heat on global economic growth, with detailed parameter estimation results provided in Table A3 of the Supplementary Material. The effect varies with regional mean annual temperatures—in relatively colder regions, increase in extreme heat tends to promote economic growth, whereas in hotter regions, it exerts adverse effects on economic growth. Notably, the turning point at which an increase in extreme heat becomes harmful to economic growth is approximately 14.1°C . This finding aligns with previous research suggesting an optimal average temperature for economic

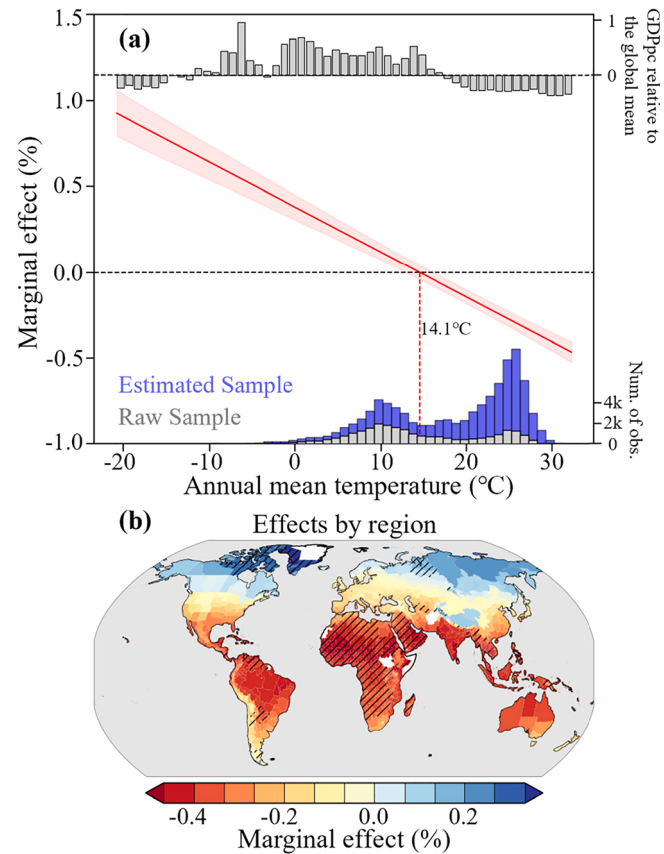


Fig. 20. Marginal effects of extreme heat on economic growth. (a) Marginal effect of extreme heat varies with regional mean temperature. GDPpc relative to the global mean is the regional GDP per capita divided by the mean of all the samples. (b) The spatial distribution of marginal effects of extreme heat. Regions with a diagonal line are those where data are completely missing in the raw sample.

growth (Burke et al., 2015; Burke et al., 2018). A beneficial marginal effect on economic growth is observed in the regions with annual mean temperature temperatures below 14.1°C , primarily in colder, high-

latitude countries. In contrast, in regions with annual mean temperature temperatures above 14.1 °C, typically warmer, low to mid-latitude countries such as those in Africa and Asia, extreme heat significantly harms economic growth. It is important to note that without comprehensive GDP data covering the majority of the globe, the identification of the marginal effect of extreme heat on global economic growth is compromised. With the original DOSE data (Wenz et al., 2023), the marginal effect of extreme heat in African regions is not available, as indicated by the diagonal line in Fig. 20b. Furthermore, our estimated data and economic loss function can be integrated into global integrated assessment models to improve forecasting accuracy (Nordhaus, 2019).

5. Conclusion

GDP per capita, as a pivotal socioeconomic indicator, plays a crucial role in evaluating potential economic damages and sustainable development challenges posed by climate change. While historical data and climate change projections have achieved remarkable coverage and resolution, both spatially and temporally, the accuracy of related assessment is often constrained by the absence of long-term, fine-grained GDP data. Official economic statistics are frequently plagued by gaps in spatial and temporal coverage, leading to unreliable estimates on the economic impacts of climate change. Grid-based remote sensing GDP datasets, often derived from national-scale economic data, encounter the issue of MAUP and lose accuracy when aggregating grids to sub-national regions. These challenges highlight the critical need for generating sub-national scale economic data to enhance the accuracy and reliability of economic assessments.

Under the modeling philosophy of spatial statistics, we developed a novel approach using deep and machine learning techniques to reconstruct the mapping relationship between VIIRS neighborhood information and DMSP data. Our models achieved considerable accuracy, with a maximum test set accuracy (correlation coefficient) of 0.98 and a minimum accuracy of above 0.945 across different continents.

Building on the premise that sub-national economic growth trends oscillate around the national economic growth trend, with the extent of fluctuations captured by variations in the intensity of sub-national NTL, we further develop a multi-layer perceptron deep learning model to derive the complex non-linear relationship between NTL and GDP per capita. The model explicitly captures both spatial clustering effects by incorporating a spatial lag term of NTL, and the regional heterogeneity effects by recognizing the hierarchical nature of data. The trained model is then applied to develop a global sub-national scale GDP per capita data spanning the past 30 years with high validation accuracy ($R=0.967$). To ensure the effectiveness and accuracy of the estimated economic data in capturing authentic economic growth patterns and depicting internal variations within countries from 1992 to 2021, we evaluate the dataset at the global, national, and sub-national scales from various angles, and the results offer solid evidence on the reliability of the estimated economic data. By linking to global climate change data, we quantify global economic losses attributed to extreme heat to demonstrate how the estimated GDP data can be useful in the climate change impact analysis.

Despite achieving high-precision estimates of global sub-national economic data, there remain instances where specific regions might be subjected to underestimation or overestimation. Moreover, the constrained temporal scope of the NTL data precludes estimates for earlier periods. Consequently, future efforts will focus on identifying suitable proxy variables with more extensive temporal series, enabling the extension of economic growth data to earlier times.

CRediT authorship contribution statement

Hang Zhang: Writing – review & editing, Writing – original draft, Visualization, Validation, Software, Resources, Methodology, Investigation, Formal analysis, Data curation, Conceptualization. **Guanpeng**

Dong: Writing – review & editing, Writing – original draft, Visualization, Validation, Supervision, Software, Resources, Project administration, Methodology, Investigation, Funding acquisition, Formal analysis, Data curation, Conceptualization. **Bing Li:** Writing – review & editing, Methodology, Conceptualization. **Zunyi Xie:** Writing – review & editing, Writing – original draft, Validation, Methodology, Conceptualization. **Changhong Miao:** Conceptualization, Methodology, Writing – review & editing. **Fan Yang:** Writing – review & editing, Methodology, Conceptualization. **Yang Gao:** Writing – review & editing, Methodology, Conceptualization. **Xiaoyu Meng:** Writing – review & editing, Methodology, Conceptualization. **Dongyang Yang:** Writing – review & editing, Methodology, Conceptualization. **Yong Liu:** Writing – review & editing, Methodology, Conceptualization. **Hongjuan Zhang:** Writing – review & editing, Methodology, Conceptualization. **Leying Wu:** Writing – review & editing, Methodology, Conceptualization. **Fanglin Shi:** Writing – review & editing, Writing – original draft, Visualization, Validation, Methodology, Data curation, Conceptualization. **Yulong Chen:** Writing – review & editing, Methodology, Conceptualization. **Wenjie Wu:** Writing – review & editing, Methodology, Conceptualization. **Edyta Laszkiewicz:** Writing – review & editing, Methodology, Conceptualization. **Yutian Liang:** Conceptualization, Methodology, Writing – review & editing. **Binbin Lu:** Writing – review & editing, Methodology, Conceptualization. **Jing Yao:** Writing – review & editing, Methodology, Conceptualization. **Xuecao Li:** Writing – review & editing, Methodology, Conceptualization.

Declaration of competing interest

The authors declare that they have no known competing financial interests or personal relationships that could have appeared to influence the work reported in this paper.

Data availability

we have shared our data and codes at <https://doi.org/10.6084/m9.figshare.24024597>

Acknowledgments

This research was funded by National Natural Science Foundation of China under Grant No. 42001115.

Appendix A. Supplementary data

Supplementary data to this article can be found online at <https://doi.org/10.1016/j.jag.2024.104086>.

References

- Bell, B., Hersbach, H., Simmons, A., Berrisford, P., Dahlgren, P., Horányi, A., Muñoz-Sabater, J., Nicolas, J., Radu, R., Schepers, D., 2021. The ERA5 global reanalysis: preliminary extension to 1950. Q. J. R. Meteorol. Soc. 147 (741), 4186–4227. <https://doi.org/10.1002/qj.4174>.
- Bennett, M.M., Smith, L.C., 2017. Advances in using multitemporal night-time lights satellite imagery to detect, estimate, and monitor socioeconomic dynamics. Remote Sens. Environ. 192, 176–197. <https://doi.org/10.1016/j.rse.2017.01.005>.
- Bhaduri, B., Bright, E., Coleman, P., Urban, M.L., 2007. LandScan USA: a high-resolution geospatial and temporal modeling approach for population distribution and dynamics. GeoJournal 69 (1), 103–117. <https://doi.org/10.1007/s10708-007-9105-9>.
- Bowen, A., Cochrane, S., Fankhauser, S., 2012. Climate change, adaptation and economic growth. Clim. Change 113 (2), 95–106. <https://doi.org/10.1007/s10584-011-0346-8>.
- Burke, M., Hsiang, S.M., Miguel, E., 2015. Global non-linear effect of temperature on economic production. Nature 527 (7577), 235–239. <https://doi.org/10.1038/nature15725>.
- Burke, M., Davis, W.M., Diffenbaugh, N.S., 2018. Large potential reduction in economic damages under UN mitigation targets. Nature 557 (7706), 549–553. <https://doi.org/10.1038/s41586-018-0071-9>.
- Carmignani, F., 2003. Political Instability, uncertainty and economics. J. Econ. Surv. 17 (1), 1–54. <https://doi.org/10.1111/1467-6419.00187>.

- Chen, T., & Guestrin, C. (2016). Xgboost: A scalable tree boosting system. *Proceedings of the 22nd ACM SIGKDD international conference on knowledge discovery and data mining*, 785–794. 10.1145/2939672.2939785.
- Chen, X., & Nordhaus, W. D. (2011). Using luminosity data as a proxy for economic statistics. *Proceedings of the National Academy of Sciences of the United States of America*, 108(21), 8589–8594. 10.1073/pnas.1017031108.
- Chen, J., Gao, M., Cheng, S., Hou, W., Song, M., Liu, X., Liu, Y., Shan, Y., 2020. County-level CO₂ emissions and sequestration in China during 1997–2017. *Sci. Data* 7 (1), 391. <https://doi.org/10.1038/s41597-020-00736-3>.
- Chen, J., Gao, M., Cheng, S., Hou, W., Song, M., Liu, X., Liu, Y., 2022. Global 1 km × 1 km gridded revised real gross domestic product and electricity consumption during 1992–2019 based on calibrated nighttime light data. *Sci. Data* 9 (1), 202. <https://doi.org/10.1038/s41597-022-01322-5>.
- Chen, Y., Liu, X., Li, X., 2017. Analyzing Parcel-Level Relationships between Urban land expansion and activity changes by integrating landsat and nighttime light data. *Remote Sens. (Basel)* 9 (2), 164. <https://doi.org/10.3390/rs9020164>.
- Chen, Z., Yu, B., Yang, C., Zhou, Y., Yao, S., Qian, X., Wang, C., Wu, B., Wu, J., 2021. An extended time series (2000–2018) of global NPP-VIIRS-like nighttime light data from a cross-sensor calibration. *Earth Syst. Sci. Data* 13 (3), 889–906. <https://doi.org/10.5194/essd-13-889-2021>.
- Cui, Y., Shi, K., Jiang, L., Qiu, L., Wu, S., 2021. Identifying and evaluating the nighttime economy in China using multisource data. *IEEE Geosci. Remote Sens. Lett.* 18, 1906–1910. <https://doi.org/10.1109/LGRS.2020.3010936>.
- Deaton, A., 2001. Counting the World's Poor: problems and Possible Solutions. *World Bank Res. Obs.* 16 (2), 125–147. <https://doi.org/10.1093/wbro/16.2.125>.
- Dong, G., Harris, R.J., 2015. Spatial Autoregressive Models for Geographically hierarchical data structures. *Geogr. Anal. Geographical Analysis* 47 (2), 173–191. <https://doi.org/10.1111/gean.12049>.
- Dong, G., Ma, J., Kwan, M.-P., Wang, Y., Chai, Y., 2018. Multi-level temporal autoregressive modelling of daily activity satisfaction using GPS-integrated activity diary data. *Int. J. Geogr. Inf. Sci.* 32 (11), 2189–2208. <https://doi.org/10.1080/13658816.2018.1504219>.
- Elvidge, C. D., Baugh, K. E., Zhizhin, M. N., & Hsu, F.-C. (2013). Why VIIRS data are superior to DMSP for mapping nighttime lights. *Proceedings of the Asia-Pacific Advanced Network*, 35, 62–69. 10.7125/APAN.35.7.
- Elvidge, C.D., Ziskin, D., Baugh, K.E., Tuttle, B.T., Ghosh, T., Pack, D.W., Erwin, E.H., Zhizhin, M., 2009. A Fifteen Year record of global natural gas flaring derived from satellite data. *Energies* 2 (3), 595–622. <https://doi.org/10.3390/en20030595>.
- Fankhauser, S., Jotzo, F., 2018. Economic growth and development with low-carbon energy. *WIREs Clim. Change* 9 (1), e495.
- Fotheringham, A.S., Wong, D.W.S., 1991. The Modifiable areal unit problem in multivariate statistical analysis. *Environment and Planning a: Economy and Space* 23 (7), 1025–1044. <https://doi.org/10.1068/a231025>.
- Geiger, T., 2018. Continuous national gross domestic product (GDP) time series for 195 countries: past observations (1850–2005) harmonized with future projections according to the Shared Socio-economic Pathways (2006–2100) [Article]. *Earth Syst. Sci. Data* 10 (2), 847–856. <https://doi.org/10.5194/essd-10-847-2018>.
- Gennaioli, N., La Porta, R., Lopez-de-Silanes, F., Shleifer, A., 2013. Human Capital and Regional Development. *Q. J. Econ.* 128 (1), 105–164. <https://doi.org/10.1093/qje/qjs050>.
- Giannetti, M., 2002. The effects of integration on regional disparities: Convergence, divergence or both? *Eur. Econ. Rev.* 46 (3), 539–567. [https://doi.org/10.1016/S0014-2921\(01\)00166-0](https://doi.org/10.1016/S0014-2921(01)00166-0).
- Goodfellow, I., Bengio, Y., Courville, A., 2016. Deep learning. MIT press.
- Henderson, J.V., Storeygard, A., Weil, D.N., 2012. Measuring economic growth from outer space. *Am. Econ. Rev.* 102 (2), 994–1028. <https://doi.org/10.1257/aer.102.2.994>.
- Hsiang, S., 2016. Climate econometrics. *Ann. Rev. Resour. Econ.* 8 (1), 43–75. <https://doi.org/10.1146/annurev-resource-100815-095343>.
- Ipcc, 2023. Climate Change 2023: Synthesis Report. Contribution of Working Groups I, II and III to the Sixth Assessment Report of the Intergovernmental Panel on Climate Change. IPCC, Geneva, Switzerland.
- Janelle, D.G., Warf, B., Hansen, K., 2004. WorldMinds: Geographical Perspectives on 100 Problems: commemorating the 100th anniversary of the Association of American Geographers 1904–2004. Springer Science & Business Media. <https://doi.org/10.1007/978-1-4613-2352-1>.
- Kalkuhl, M., Wenz, L., 2020. The impact of climate conditions on economic production. Evidence from a global panel of regions. *J. Environ. Econ. Manag.* 103, 102360. <https://doi.org/10.1016/j.jeem.2020.102360>.
- Ke, G., Meng, Q., Finley, T., Wang, T., Chen, W., Ma, W., Ye, Q., & Liu, T.-Y. (2017). LightGBM: a highly efficient gradient boosting decision tree Proceedings of the 31st International Conference on Neural Information Processing Systems, Long Beach, California, USA.
- Kotz, M., Wenz, L., Stechemesser, A., Kalkuhl, M., Levermann, A., 2021. Day-to-day temperature variability reduces economic growth. *Nat. Clim. Chang.* 11 (4), 319–325. <https://doi.org/10.1038/s41558-020-00985-5>.
- Kummu, M., Taka, M., Guillaume, J.H.A., 2018. Gridded global datasets for Gross Domestic Product and Human Development Index over 1990–2015. *Sci. Data* 5 (1), 180004. <https://doi.org/10.1038/sdata.2018.4>.
- Kunkel, K.E., Pielke, R.A., Changnon, S.A., 1999. Temporal Fluctuations in Weather and climate extremes that cause economic and human health impacts: a review. *Bull. Am. Meteorol. Soc.* 80 (6), 1077–1098. [https://doi.org/10.1175/1520-0477\(1999\)080<1077:TFIWAC>2.0.CO;2](https://doi.org/10.1175/1520-0477(1999)080<1077:TFIWAC>2.0.CO;2).
- Kuznets, S.S., 1955. Economic Growth and Income Inequality. *Am. Econ. Rev.* 45 (1), 1–28. <https://doi.org/10.4324/9780429311208-4>.
- Li, X., Zhou, Y., Zhao, M., Zhao, X., 2020. A harmonized global nighttime light dataset 1992–2018. *Sci. Data* 7 (1), 168. <https://doi.org/10.1038/s41597-020-0510-y>.
- Liu, H., Wang, L., Sherman, D., Gao, Y., Wu, Q., 2010. An object-based conceptual framework and computational method for representing and analyzing coastal morphological changes. *Int. J. Geogr. Inf. Sci.* 24 (7), 1015–1041. <https://doi.org/10.1080/13658810903270569>.
- Lundberg, S.M., Lee, S.-I., 2017. A unified approach to interpreting model predictions. In: *Advances in Neural Information Processing Systems*, p. 30.
- McCord, G.C., Rodriguez-Heredia, M., 2022. Nightlights and Subnational Economic Activity: Estimating Departmental GDP in Paraguay. *Remote Sens. (Basel)* 14 (5), 1150. <https://doi.org/10.3390/rs14051150>.
- Nechaev, D., Zhizhin, M., Poyda, A., Ghosh, T., Hsu, F.-C., Elvidge, C., 2021. Cross-Sensor Nighttime lights image calibration for DMSP/OLS and SNPP/VIIRS with Residual U-Net. *Remote Sens. (Basel)* 13 (24), 5026. <https://doi.org/10.3390/rs13245026>.
- Nordhaus, W.D., 1991. Economic approaches to greenhouse warming. *Economic policy responses, Global warming*, pp. 33–68.
- Nordhaus, W., 2019. Climate Change: the Ultimate Challenge for Economics. *Am. Econ. Rev.* 109 (6), 1991–2014. <https://doi.org/10.1257/aer.109.6.1991>.
- Otto, I.M., Biewald, A., Coumou, D., Feulner, G., Köhler, C., Nocke, T., Blok, A., Gröber, A., Selchow, S., Tyfield, D., Volkmer, I., Schellnhuber, H.J., Beck, U., 2015. Socio-economic data for global environmental change research. *Nat. Clim. Chang.* 5 (6), 503–506. <https://doi.org/10.1038/nclimate2593>.
- Pinkovskiy, M., Sala-i-Martin, X., 2016. Lights, Camera Income! Illuminating the National Accounts-Household Surveys Debate. *Q. J. Econ.* 131 (2), 579–631. <https://doi.org/10.1093/qje/qjw003>.
- Sánchez de Miguel, A., Zamorano, J., Aubé, M., Bennie, J., Gallego, J., Ocaña, F., Pettit, D.R., Stefanov, W.L., Gaston, K.J., 2021. Colour remote sensing of the impact of artificial light at night (II): Calibration of DSLR-based images from the International Space Station. *Remote Sens. Environ.* 264, 112611. <https://doi.org/10.1016/j.rse.2021.112611>.
- Shi, K., Chen, Y., Yu, B., Xu, T., Yang, C., Li, L., Huang, C., Chen, Z., Liu, R., Wu, J., 2016. Detecting spatiotemporal dynamics of global electric power consumption using DMSP-OLS nighttime stable light data. *Appl. Energy* 184, 450–463. <https://doi.org/10.1016/j.apenergy.2016.10.032>.
- K. Shi J. Ma Z. Chen Y. Cui B. Yu Nighttime light remote sensing in characterizing urban spatial structure. *The Innovation Geoscience* 1(3), 100043 2023 10.59717/j.xinngeo.2023.100043.
- Srivastava, N., Hinton, G., Krizhevsky, A., Sutskever, I., Salakhutdinov, R., 2014. Dropout: a simple way to prevent neural networks from overfitting. *J. Mach. Learn. Res.* 15 (1), 1929–1958.
- Su, H., Wang, A., Zhang, T., Qin, T., Du, X., Yan, X.-H., 2021. Super-resolution of subsurface temperature field from remote sensing observations based on machine learning. *Int. J. Appl. Earth Obs. Geoinf.* 102, 102440. <https://doi.org/10.1016/j.jag.2021.102440>.
- Tatem, A.J., 2017. WorldPop, open data for spatial demography. *Sci. Data* 4 (1), 170004. <https://doi.org/10.1038/sdata.2017.4>.
- Thorsen-Meyer, H.-C., Placido, D., Kaas-Hansen, B.S., Nielsen, A.P., Lange, T., Nielsen, A. B., Toft, P., Schierbeck, J., Strom, T., Chmura, P.J., Heimann, M., Belling, K., Perner, A., Brunak, S., 2022. Discrete-time survival analysis in the critically ill: a deep learning approach using heterogeneous data. *npj Digital Med.* 5 (1), 142. <https://doi.org/10.1038/s41746-022-00679-6>.
- Townsend, A.C., Bruce, D.A., 2010. The use of night-time lights satellite imagery as a measure of Australia's regional electricity consumption and population distribution. *Int. J. Remote Sens.* 31 (16), 4459–4480. <https://doi.org/10.1080/01431160903261005>.
- Wang, T., Sun, F., 2022. Global gridded GDP data set consistent with the shared socioeconomic pathways. *Sci. Data* 9 (1), 221. <https://doi.org/10.1038/s41597-022-01300-x>.
- Wenz, L., Carr, R.D., Kögel, N., Kotz, M., Kalkuhl, M., 2023. DOSE – Global data set of reported sub-national economic output. *Sci. Data* 10 (1), 425. <https://doi.org/10.1038/s41597-023-02323-8>.
- Wooldridge, J.M., 2010. *Econometric analysis of cross section and panel data*. MIT press.
- Wu, Y., Shi, K., Chen, Z., Liu, S., Chang, Z., 2022. Developing Improved Time-Series DMSP-OLS-Like Data (1992–2019) in China by Integrating DMSP-OLS and SNPP-VIIRS. *IEEE Trans. Geosci. Remote Sens.* 60, 1–14. <https://doi.org/10.1109/TGRS.2021.3135333>.
- Xie, Z., Zhao, Y., Jiang, R., Zhang, M., Hammer, G., Chapman, S., Brider, J., Potgieter, A. B., 2024. Seasonal dynamics of fallow and cropping lands in the broadacre cropping region of Australia. *Remote Sens. Environ.* 305, 114070. <https://doi.org/10.1016/j.rse.2024.114070>.
- Yang, C., Yu, B., Chen, Z., Song, W., Zhou, Y., Li, X., Wu, J., 2019. A Spatial-Socioeconomic urban development status curve from NPP-VIIRS Nighttime Light Data. *Remote Sens. (Basel)* 11 (20), 2398. <https://doi.org/10.3390/rs11202398>.
- Yu, B., Shi, K., Hu, Y., Huang, C., Chen, Z., Wu, J., 2015. Poverty Evaluation Using NPP-VIIRS nighttime light composite data at the county level in china. *IEEE J. Sel. Top. Appl. Earth Obs. Remote Sens.* 8 (3), 1217–1229. <https://doi.org/10.1109/JSTARS.2015.2399416>.
- Yu, B., Tang, M., Wu, Q., Yang, C., Deng, S., Shi, K., Peng, C., Wu, J., Chen, Z., 2018. Urban Built-Up Area extraction from log-transformed NPP-VIIRS Nighttime Light composite data. *IEEE Geosci. Remote Sens. Lett.* 15 (8), 1279–1283. <https://doi.org/10.1109/LGRS.2018.2830797>.
- Zhang, H., Dong, G., Wang, J., Zhang, T.-L., Meng, X., Yang, D., Liu, Y., Lu, B., 2023. Understanding and extending the geographical detector model under a linear regression framework. *Int. J. Geogr. Inf. Sci.* 37 (11), 2437–2453. <https://doi.org/10.1080/13658816.2023.2266497>.

- Zhang, Q., Seto, K.C., 2011. Mapping urbanization dynamics at regional and global scales using multi-temporal DMSP/OLS nighttime light data. *Remote Sens. Environ.* 115 (9), 2320–2329. <https://doi.org/10.1016/j.rse.2011.04.032>.
- Zheng, Q., Weng, Q., Wang, K., 2019. Developing a new cross-sensor calibration model for DMSP-OLS and Suomi-NPP VIIRS night-light imageries. *ISPRS J. Photogramm. Remote Sens.* 153, 36–47. <https://doi.org/10.1016/j.isprsjprs.2019.04.019>.
- Zheng, Q., Seto, K.C., Zhou, Y., You, S., Weng, Q., 2023. Nighttime light remote sensing for urban applications: progress, challenges, and prospects. *ISPRS J. Photogramm. Remote Sens.* 202, 125–141. <https://doi.org/10.1016/j.isprsjprs.2023.05.028>.
- Zhou, Y., Smith, S.J., Elvidge, C.D., Zhao, K., Thomson, A., Imhoff, M., 2014. A cluster-based method to map urban area from DMSP/OLS nightlights. *Remote Sens. Environ.* 147, 173–185. <https://doi.org/10.1016/j.rse.2014.03.004>.
- Zhou, Y., Chen, M., Tang, Z., Zhao, Y., 2022. City-level carbon emissions accounting and differentiation integrated nighttime light and city attributes. *Resour. Conserv. Recycl.* 182, 106337 <https://doi.org/10.1016/j.resconrec.2022.106337>.